

UC San Diego

UC San Diego Previously Published Works

Title

Design, synthesis, and biological activity of substituted 2-amino-5-oxo-5H-chromeno[2,3-b]pyridine-3-carboxylic acid derivatives as inhibitors of the inflammatory kinases TBK1 and IKK ϵ for the treatment of obesity

Permalink

<https://escholarship.org/uc/item/3xt4k1zq>

Journal

Bioorganic & Medicinal Chemistry, 26(20)

ISSN

0968-0896

Authors

Beyett, Tyler S
Gan, Xinmin
Reilly, Shannon M
et al.

Publication Date

2018-11-01

DOI

10.1016/j.bmc.2018.09.020

Peer reviewed



Published in final edited form as:

Bioorg Med Chem. 2018 November 01; 26(20): 5443–5461. doi:10.1016/j.bmc.2018.09.020.

Design, synthesis, and biological activity of substituted 2-amino-5-oxo-5H-chromeno[2,3-b]pyridine-3-carboxylic acid derivatives as inhibitors of the inflammatory kinases TBK1 and IKK ϵ for the treatment of obesity

Tyler S. Beyett^{#a,b}, Xinmin Gan^{#c,d}, Shannon M. Reilly^e, Andrew V. Gomez^e, Louise Chang^b, John J. G. Tesmer^b, Alan R. Saltiel^e, and Hollis D. Showalter^{c,d}

^aProgram in Chemical Biology, Departments of Pharmacology and Biological Chemistry, University of Michigan, Ann Arbor, MI 48109, United States

^bLife Sciences Institute, Departments of Pharmacology and Biological Chemistry, University of Michigan, Ann Arbor, MI 48109, United States

^cDepartment of Medicinal Chemistry, University of Michigan, Ann Arbor, MI 48109, United States

^dVahlteich Medicinal Chemistry Core, University of Michigan, Ann Arbor, MI 48109, United States

^eDepartments of Medicine and Pharmacology, Institute for Diabetes and Metabolic Health, University of California, San Diego, La Jolla, CA 92093-0912, United States

These authors contributed equally to this work.

Abstract

The non-canonical I κ B kinases TANK-binding kinase 1 (TBK1) and inhibitor of nuclear factor kappa-B kinase ϵ (IKK ϵ) play a key role in insulin-independent pathways that promote energy storage and block adaptive energy expenditure during obesity. Utilizing docking calculations and the x-ray structure of TBK1 bound to amlexanox, an inhibitor of these kinases with modest potency, a series of analogues was synthesized to develop a structure activity relationship (SAR) around the A- and C-rings of the core scaffold. A strategy was developed wherein R₇ and R₈ A-ring substituents were incorporated late in the synthetic sequence by utilizing palladium-catalyzed cross-coupling reactions on appropriate bromo precursors. Analogues display IC₅₀ values as low as 210 nM and reveal A-ring substituents that enhance selectivity toward either kinase. In cell assays, selected analogues display enhanced phosphorylation of p38 or TBK1 and elicited IL-6 secretion in 3T3-L1 adipocytes better than amlexanox. An analogue bearing a R₇ cyclohexyl modification demonstrated robust IL-6 production in 3T3-L1 cells as well as a phosphorylation marker of efficacy and was tested in obese mice where it promoted serum IL-6 response, weight

Correspondence to: Hollis D. Showalter.

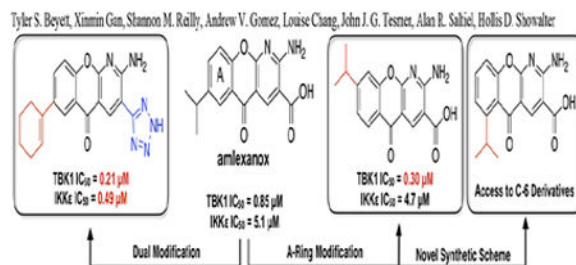
Publisher's Disclaimer: This is a PDF file of an unedited manuscript that has been accepted for publication. As a service to our customers we are providing this early version of the manuscript. The manuscript will undergo copyediting, typesetting, and review of the resulting proof before it is published in its final citable form. Please note that during the production process errors may be discovered which could affect the content, and all legal disclaimers that apply to the journal pertain.

Supplementary material

Supplementary material associated with this article can be found, in the online version, at xxx.

loss, and insulin sensitizing effects comparable to amlexanox. These studies provide impetus to expand the SAR around the amlexanox core toward uncovering analogues with development potential.

Graphical Abstract



Keywords

obesity; amlexanox; TANK-binding kinase 1 (TBK1); inhibitor of nuclear factor kappa-B kinase subunit epsilon (IKK ϵ); TBK1·amlexanox co-crystal; SAR

1. Introduction

The current worldwide epidemic of obesity is exacting profound human health costs in both industrialized and developing nations, where it is associated with an increased risk of developing a host of medical conditions such as type 2 diabetes, dyslipidemia, non-alcoholic fatty liver disease, cardiovascular disease, and cancer.[1] As of 2015, one-third of adults in the United States were obese and an additional one-third overweight.

The mechanisms by which obesity can lead to type 2 diabetes and other diseases remain unresolved, and little progress has been made in devising new therapeutic strategies that attack the core defects underlying either disorder.[2] The few pharmacological therapies available for the treatment of obesity act principally through the central nervous system, but provide only modest suppression of appetite at therapeutically viable doses.[3] In some treatments, a combination of medications that intervene by more than one biochemical pathway is utilized.[4] Exemplary small molecule drugs are (i) a combination of phentermine (1), a sympathomimetic amine that acts as an appetite suppressant and stimulant, and topiramate (2) an anticonvulsant[1]; (ii) lorcaserin (3), a selective 5-HT_{2C} receptor agonist[5]; and (iii) orlistat (4), which blocks fat absorption in the intestine by acting as a lipase inhibitor [6] (Figure 1). Beyond that, there is little new in development. Indeed, none of the currently available and widely used treatments for obesity addresses the underlying energy imbalance that is the root cause.[7]

One hallmark of obesity is a state of chronic, low-grade inflammation in liver and fat tissue. Prior studies on the inflammatory links between obesity and type 2 diabetes led to the elucidation of an important role for the nuclear factor kappa-light-chain-enhancer of activated B cells (NF- κ B) pathway, revealing the role of two non-canonical inhibitors of kappa B (I κ B) kinases, TANK-binding kinase 1 (TBK1) and inhibitor of nuclear factor

kappa-B kinase subunit ϵ (IKK ϵ), in insulin-independent pathways that promote energy storage and block adaptive energy expenditure during obesity.[8] The expression and activity of these kinases are increased in mice fed a high fat diet due to the generation of inflammation in response to obesity. Deletion of the IKK ϵ gene attenuated some of the deleterious metabolic effects of high fat feeding including reduced weight gain, lowered insulin resistance, and less chronic low-grade inflammation. These data led to a new hypothesis about the role of inflammation in the generation of insulin resistance and type 2 diabetes during obesity,[9] prompting a high-throughput screen for small molecule inhibitors of the TBK1 and IKK ϵ kinases. One hit from the screen was amlexanox (**5**; Figure 1), an approved drug for the treatment of canker sores, asthma, and allergic rhinitis. The compound proved to be a modest inhibitor of TBK1 and IKK ϵ and reproduced the effects of the IKK ϵ knockout phenotype, which include weight loss in obese mice, improved insulin sensitivity, and reduced hepatic steatosis and inflammation. Amlexanox also increased the level of the second messenger molecule cAMP and triggered the release of the hormone interleukin-6 (IL-6) from fat cells thereby reducing the production of glucose. Two recent clinical trials indicated that amlexanox treatment effectively lowered glycated hemoglobin (HbA1c) in a subset of patients with obesity and type 2 diabetes.[10]

Amlexanox is thus an attractive starting point for analogue synthesis. We previously reported the TBK1-amlexanox structure which revealed the amino pyridine moiety on amlexanox binding the kinase hinge in a canonical type 1, DFG-in mode.[11] The C-3 carboxylic acid interacts with Thr156, and its replacement with acid bioisosteres improved the potency of amlexanox but without improvement in efficacy. In this paper, we detail the synthesis of core modifications of amlexanox and develop a more detailed structure-activity relationship (SAR) that addresses some of the liabilities of amlexanox, including its modest potency and low solubility. We also report the X-ray co-crystal structures of select amlexanox analogues and TBK1, which will guide our future studies toward generating analogues with enhanced potency and selectivity.

2. Analogue Design

We first focused on modifications around the A ring of amlexanox and designed a set of analogues bearing conservative modifications at the C-7 position alongside a small set of C-6 and C-8 derivatives that may stabilize the phosphate-binding loop (P-loop) or interact with the kinase hinge, respectively. Next, a large series of cyclic modifications were examined at the C-7 position due to their synthetic accessibility and in consideration of the crystallographic data showing space to accommodate bulkier modifications. Finally, previously reported bioisostere derivatives of the C-3 carboxylic acid[11] were combined with C-7 modifications to assess the effect of dual modification of the pharmacophore.

3. Chemistry

Synthetic methodologies to make amlexanox and analogues were reported several decades ago by Takeda investigators.[12], [13], [14] In almost all cases, the A-ring substituent had been incorporated early onto a precursor 4-oxo-4*H*-1-benzopyran-3- carbonitrile. With a goal to develop a more efficient route for higher output of analogues, we mapped out a strategy of

introducing A-ring substituents at a later stage of the synthetic sequence. Our overall strategy is outlined in Scheme 1, wherein suitable tricyclic A-ring bromo-substituted precursors (**6** – **10**; Scheme 1) were first synthesized and then subjected to a range of palladium-catalyzed cross-coupling reactions (carbon-carbon, carbon-nitrogen) to introduce a broad range of R6–R8 functionality. The resultant ethyl ester intermediates (**15–24**, **32–58**) with olefinic/alkynic side chains would then be reduced via catalytic hydrogenation to products (**25** – **31**, **59** – **84**) embellished with a wide variety of side chains. Subsequent base hydrolysis of these and selected unsaturated precursors, along with a few amine congeners generated from Buchwald coupling, would then provide a broad range of analogues (Tables 1 and 2) for initial evaluation in our enzyme assays. These were supplemented with a smaller set of congeners with a tetrazole bioisostere installed in the C-3 position of the C-ring (Table 3).

The synthesis of novel tricyclic precursors **6–8** followed a fairly classical sequence of reactions starting with commercially available bromo- substituted (2-hydroxyaryl)ethan-1-ones (**11a** – **11c**; Scheme 2). Hence, treatment of **11a** or **11b** with a large excess of Vilsmeier reagent resulted in a two-stage homologation to give 7- or 6-bromo-4-oxo-4*H*-chromene-3-carbaldehydes **12a** and **12b**, respectively, in 73 – 88% yield. Homologation of 2-bromo-5-hydroxypyridin-4-yl)ethan-1-one[15] (**11c**) could not be achieved under these conditions, thus an alternate approach was taken. Treatment of **11c** with Brederick's reagent proceeded smoothly to generate intermediate (*E*)-1-(2-bromo-5-hydroxypyridin-4-yl)-3-(dimethylamino)prop-2-en-1-one in 60% yield following chromatography. Further homologation using Vilsmeier reagent derived from DMF and triflic anhydride then provided 6-bromo-4-oxo-4*H*-pyrano[2,3-*c*]pyridine-3-carbaldehyde (**12c**) in 88% yield. The use of Vilsmeier reagent with the weakly nucleophilic triflate counterion was critical to the success of this reaction. Further elaboration of carbaldehydes **12a** – **12c** to corresponding oximes **13a** – **13c** and then nitriles **14a** – **14c** employed conditions utilized for the synthesis of related 4-oxo-4*H*-chromenes. Annulation of nitriles **14a** – **14c** with ethyl cyanoacetate to tricyclic starting materials **6** – **8** of Scheme 1 was achieved in 77 – 93% yield utilizing literature conditions. Compound **9** was synthesized as previously described[16] and converted to *N*-Boc derivative **10** in 83% yield.

The synthesis of targeted 7- or 8-(substituted)-5-oxo-5*H*-chromeno[2,3-*b*]pyridine-3-carboxylic acids and 8-aza congeners along with unsaturated precursors, following the strategy outlined in Scheme 1, is shown in detail in Schemes SM1 and SM2 (Supplementary Materials). After considerable experimentation, we determined that N-2 unprotected amines were optimal for Suzuki[17] or Sonogashira[18] couplings. Thus treatment of **6** – **9** with a wide range of alk/cycloalk-1-en-1-ylboronic acids or 2-(alk/cycloalk-1-en-1-yl)-4,4,5,5-tetramethyl-1,3,2-dioxaborolanes under standard Suzuki conditions provided alkene products (**15** – **18**, **24**, Scheme SM1; **36** – **52**, **55** – **58**, Scheme SM2) in 61–95% yield. Similarly, Sonogashira reaction of **9** with selected substituted alk-1-ynes provided alkyne adducts (**19** – **21**, Scheme SM1; **53**, **54**, Scheme SM2) in 67–94% yield. However, Suzuki coupling to derive cyclopropyl adduct **32** necessitated starting with *N*-Boc-protected **10**, which was also required for Negishi cross-coupling[19] of isobutyl and *c*-butylzinc bromides to give adducts **22** and **34**, respectively. The *N*-Boc protecting group of each was cleaved

with TFA to give the respective products **33**, **23**, and **35**. Hydrogenation of unsaturated esters (**15 – 17**, **19 – 21**, **24**, Scheme SM1; **36 – 39**, **41 – 52**, **54 – 58**, Scheme SM2) over 10% palladium on carbon proceeded smoothly to give corresponding saturated R₇/R₈ derivatives in modest to excellent yields. Ester hydrolysis of these (and **62**, **71– 73**, **76** derived from further transformations), along with selected precursor R₇ and R₈ alkenes/alkynes, under standard base conditions provided the corresponding linear (**105–107**, **109–112**, **114–121**, Scheme SM1: Table 1) and cyclic (**122–150**, **152–167**, Scheme SM2; Table 2) amlexanox analogues in 48 – 95% yield.

The synthesis of the C-6 isomer of amlexanox (**108**; Scheme 3) could not be achieved via the pathway outlined above for R₇/R₈ congeners. Standard Vilsmeier homologation of **85** provided chromone carbaldehyde **86** in 94% yield with further transformations to oxime **87** (77% yield) and nitrile **88** (99% yield) proceeding uneventfully. However, attempted annulation of **88** with ethyl cyanoacetate toward securing tricyclic C-6 bromide under conditions providing **6–9** could not be achieved. Therefore, a different ordering of steps to install the C-6 isopropyl side chain was investigated. The application of standard Suzuki conditions to **88** resulted in complete destruction, due to its exquisite sensitivity to base, whereas a milder Stille cross-coupling[20] reaction *in the absence of base* gave **89** in 81% yield. This was then parlayed into targeted C-6 amlexanox (**108**, Table 1) in three standard steps in 49% overall yield. Scheme 3 also outlines alternative reaction manifolds toward securing **108** via Suzuki-derived intermediate **92**. Subsequent reactions to intermediate aldehydes **93** and **95** proceeded smoothly, but attempted oximation of each surprisingly resulted in compound destruction.

The synthesis of selected R₇ amino analogues of amlexanox is delineated in Scheme 4A. The R₇ amine moiety was efficiently installed in the first step from **96** using Buchwald palladium catalyzed cross-coupling conditions[21] to give **97a,b**. Applying similar conditions [22] to tricyclic bromide **10** did not provide product. Application of a sequence of standard steps (Vilsmeier homologation, nitrile formation, and annulation) to **97a,b** then gave ester intermediates (**100 a,b**), which were hydrolyzed under basic conditions to target carboxylic acids (**113**, Table 1; **151**, Table 2).

A final set of analogues was synthesized incorporating tetrazole into the R₃ position as a carboxylic acid bioisostere (Scheme 4B). Toward this end, tricyclic bromo nitrile **101** was elaborated via Suzuki chemistry to R₇ cyclohexene derivative **102**, which was then saturated to **103** by catalytic hydrogenation. Each of these was elaborated into its respective R₃ tetrazole under standard conditions (sodium azide, ammonium chloride, DMF) to provide **169** and **168**, respectively (Table 3). Similarly, bicyclic nitriles **99a,b** were annulated into tricyclic R₃ nitriles **104a,b**, which were then transformed to R₇ (dialkylamino)-substituted R₃- tetrazoles **170** and **171**, respectively (Table 3). A final target was made via Schotten-Bauman acylation of carboxylic acid **151** to give R₇-morpholinyl, R₃-tetrazole amide analogue **172** (Table 3).

All compounds were rigorously purified by flash chromatography or crystallization, and their structural assignments are supported by diagnostic peaks in the ¹H NMR spectra and by mass spectrometry. Digital copies of NMR spectra can be found in Supplementary

Materials. The reagents utilized in reactions to our target compounds are summarized in the legends of Schemes 2–4 and Schemes SM1 and SM2 (Supplementary Materials). All reactions are categorized according to generalized Methods A – N, and experimental procedures for each are organized accordingly in the Experimental Section. Representative experimental procedures are given for the Suzuki reaction (Method A), catalytic hydrogenation (Method D), and base hydrolysis (Method E). Additional procedures for compounds derived from these three methods are provided in Supplemental Materials.

4. Kinase inhibition

All the compounds in Tables 1–3 were investigated for inhibition of recombinant human TBK1 and IKK ϵ . The IC₅₀ values shown were determined by dose-response radiometric kinase assays with myelin basic protein as substrate, and are technically apparent IC₅₀ values. Each is an average of three separate determinations.

Selected analogues in Tables 1–3 bearing more extensive A-ring modifications, which may dramatically affect potency, were first evaluated at a single concentration of 1 or 5 μ M. This approximately corresponds to the IC₅₀ of amlexanox (**5**) toward TBK1 and IKK ϵ , respectively. Based on their % inhibition relative to amlexanox, full dose-response assays were conducted. Most of these compounds are shown in Tables 2 and 3.

Table 1 lists the structures and kinase inhibitory properties of a series of linear alkyl, alkenyl, and alkynyl A-ring derivatives of amlexanox (**5**), which is used for comparison. Analogues bearing a 2-propenyl substituent at R₇ (**105**, **110**, **112**) or R₈ (**107**) generally show reduced potency toward TBK1 and improved potency toward IKK ϵ when located at the R₇ position. The addition of a methylene spacer(s) (**116**, **117**) had no significant effect on potency. The introduction of an alkyne spacer (**118**) markedly reduced potency with the data likely compromised due to poor solubility in the assay medium. To improve the solubility of **5**, the isopropyl group was replaced with a dimethylamino moiety in **113** which improved potency 2- and 3-fold toward TBK1 and IKK ϵ , respectively.

Moving the isopropyl group to the C-6 position (**108**) in an attempt to stabilize the P-loop by packing against Leu15 and Gly16, reduced potency toward TBK1 without affecting potency toward IKK ϵ . The introduction of fluorine at the R₈ position (**109**) enhanced potency toward TBK1 relative to amlexanox (**5**), whereas the 2-propenyl congener (**110**) was essentially equivalent for TBK1 but enhanced for IKK ϵ , similar to non-fluorinated congener (**105**). Installation of a nitrogen in place of carbon at the 8-position of amlexanox to give **111** enhanced potency toward both kinases. In contrast, making the same replacement for the R₇ 2-propenyl congener **105** to give **112** negated the potency boost of the 2-propenyl substituent toward IKK ϵ .

The vast majority of synthesized analogues, incorporating R₇ and R₈ cycloalkyl, heterocyclic and alkylcycloalkyl substituents displayed decreased inhibition of both kinases relative to amlexanox (Table 2). Analogues displaying equivalent or improved inhibition were further tested in dose-response assays. Introduction of conformational restriction in amlexanox (**5**) to give cyclopropyl analogue **122** resulted in reduced potency toward both

kinases. A general decrease in inhibition was observed as the ring size at the R₇ position was increased from cyclobutyl to cycloheptyl (**123** – **125**, and **127**, respectively) with TBK1 inhibition the most adversely affected. Notably, unsaturation of the cyclohexyl ring (**126**) markedly improved inhibition of IKK ϵ relative to **125**, consistent with the prior observation for the unsaturated 2-propenyl substituent preferentially improving IKK ϵ inhibition. Further modification of the **125**, **126** pair to incorporate R₈ fluorination (**152**, **153**, respectively) or 8-aza (**154**, **155**, respectively) generally decreased inhibition toward both kinases, especially IKK ϵ . For a series of R₇ (**156** – **161**, **164**–**167**) and R₈ (**162**, **163**) analogues bearing saturated rings joined to the core through short linkers (ethane, ethene, ethyne), all were poor inhibitors of either kinase, likely due to limited solubility under the assay conditions. Installation of cyclohexyl (**128**) or cyclohexenyl (**129**) at R₈ diminished inhibition likely due to the introduction of steric clashes with the kinase hinge.

Based on preliminary cellular and *in vivo* results with **125** (*vide infra*), we extended our SAR to elaborated R₇ cyclohexyl and, in selected cases, precursor olefin analogues. All modifications were made on the distal position of the 6-membered ring substituent. Thus, *gem*-difluoro (**131**, **132**), methyl (**133**), trifluoromethyl (**134**, **135**), and *gem*-dimethyl (**136**, **137**) modifications decreased compound solubility that resulted in reduced inhibition. Hydroxylation (**138**, **139**) also reduced potency. Surprisingly, installation of distal ketone (**140**) and spiroketal (**141**) functions improved potency toward both kinases whereas the unsaturated congener of spiroketal (**142**) only significantly improved potency toward IKK ϵ .

Next, a series of analogues containing R₇ nitrogen, oxygen, and sulfur heterocycles was evaluated. The installation of a piperidinyl group at (**143**, **144**) reduced inhibition toward both kinases whereas formylation (**145**) or acetylation (**146**) of the heterocyclic nitrogen of **143** modestly improved potency toward both kinases. The installation of a tetrahydropyranyl group (**147**) had no significant effect on potency but its olefinic congener (**148**) improved potency toward IKK ϵ . In contrast, replacement of oxygen in **147** with sulfur (**149**) improved potency toward both kinases, although no improvement was observed for the sulfone congener **150**. The morpholinyl analogue **151** displayed a decrease in inhibition toward TBK1 and was essentially inactive toward IKK ϵ .

Analogues incorporating the carboxylic acid tetrazole bioisostere at the R₃ position are shown in Table 3. The combination of R₃ tetrazole and R₇ cyclohexyl moieties in **168** displayed the same potency toward TBK1 as its R₃ carboxylic acid congener **125** (Table 2), whereas its potency toward IKK ϵ significantly increased. The olefin congener (**169**) exhibited a >20-fold increase in potency toward IKK ϵ to 210 nM, consistent with prior observations that IKK ϵ favors unsaturated substituents at R₇. Significant increases in potency were also observed for the dimethylamine (**170**) and morpholinyl (**171**, **172**) analogues bearing R₃ tetrazole or amide-linked tetrazole modifications. Interestingly, **171** is a potent (310 nM) inhibitor of IKK ϵ despite its carboxylic acid congener **151** (Table 2) showing no inhibitory effect, suggesting that the tetrazole moiety is the primary driver of potency in this subclass of analogues.

5. Crystallographic studies with select analogues

To verify the binding mode of analogues, select inhibitors were co-crystallized with TBK1 (Figure 2, Table SM1). To represent the series of analogues with extended non-cyclic R₇ modifications, such as **117** and **120**, the more soluble analogue **114** was co-crystallized with TBK1 and the structure determined to 3.19 Å spacings (PDB entry 6CQ0, Figure 2A). The core of the inhibitor binds identically to amlexanox along the kinase hinge. Weak density is observed for the dimethylamino tail positioned near Pro90 and Cys91. The placement of the R₇ tail in solvent may explain why no significant changes in potency are observed, however these analogues are generally less soluble which may also contribute to a reduction in potency. The placement of the tail near Cys91, which is likely in the thiolate form due to its proximity to Arg143, suggests that incorporation of an acrylamide in place of the dimethylamine in **114** may serve as a strategy for covalent inhibitor design targeting Cys91. To represent cyclic R₇ analogues, we determined the structure of TBK1 in complex with **131** at 3.2 Å and **150** at 3.35 Å (PDB entries 6CQ4 and 6CQ5, respectively, Figure 2B-C). Both compounds bind along the hinge similar to amlexanox and the R₇ rings extend into solvent between the kinase and dimerization domains of TBK1. The lack of interaction between the *gem*-difluorocyclohexyl modification in **131** and TBK1, and decreased solubility, explains why this analogue displays decreased inhibition of both kinases. The sulfone-containing ring on **150** also does not interact with the kinase domain but is within range of Lys567 and Lys568 on the dimerization domain, which would form favorable electrostatic interactions with the sulfone group.

6. Cell studies in 3T3-L1 adipocytes

To determine the efficacy of amlexanox analogues in cellular assays, we monitored phosphorylation of p38 or TBK1 as well as secretion of IL-6 in 3T3-L1 adipocytes, which are biomarkers of TBK1 and IKK ϵ inhibition.[23] TBK1 phosphorylation is increased as the result of the blockade of a negative feedback loop involving AMPK and its target ULK1, which directly phosphorylates TBK1[24]. Phosphorylation and activation of p38 occur as a result of de-repression of cAMP levels through reduced activation of phosphodiesterase 3B (PDE-3B) by TBK1 and IKK ϵ . [23] IL-6 secretion is not only a marker of the efficacy of TBK1/IKK ϵ inhibition and p38 activation in adipocytes, but is also part of the biological response that confers metabolic benefit *in vivo*. [25] An example of the western blots used to determine phosphorylation levels is provided in Figure SM1. Enhanced phosphorylation of p38 relative to amlexanox (**5**) is observed for the C-6 isomer **108** and R₇ isobutyl homolog **116**, whereas the R₈ isomer **106** and 8-fluoro congener **109** show essentially equivalent activity to amlexanox (**5**). Surprisingly, the 8-N congener of amlexanox (**111**) is almost completely non-stimulatory, perhaps due to altered cell permeability. For TBK1 phosphorylation, the SAR is more mixed with optimal enhancement by the R₇ isopentyl homologue **117** and cyclohexyl analogue **125**. Additional enhancement was elicited by the R₇ 2-propenyl compound **105**, C-8 isomer **106**, R₈ fluoro congener **109**, unsaturated pyran (**148**) and thiopyran (**149**) analogues. In 3T3-L1 adipocytes, a number of analogues (**105**, **108**, **109**, **110**, **116**, **117**, **125**, **148**, and **149**) were found to elicit IL-6 secretion as good as, or better than, amlexanox. For these, only **108** and **116** also increased p38 phosphorylation

whereas **105**, **108**, **109**, **117**, and **148** additionally exhibited increased TBK1 phosphorylation. Analogues **125** and **149** elicited an improved response in all three readouts.

7. Computed properties and aqueous solubility

A balance between lipophilicity and aqueous solubility are key parameters that influence success in a standard oral, low-dose drug discovery program. Toward assessing drug-like properties relating to oral absorption for our series of inhibitors, lipophilic ligand efficiency (LLE) and solubility forecast indicator (SFI) calculators were utilized to derive computed values for compounds in Table 4. Using cLogP and IC₅₀ data, calculations of LLE can be calculated which provide a measure of a compound's lipophilicity associated with potency. [26],[27] That, along with SFI calculations[28] derived from cLogD_{7.4} information, provide valuable information regarding a compound's potential to be a drug. The data are shown in Table SM2, with equations for LLE and SFI calculations given in the footnotes. Computed LLE values range from 4.77 – 1.30 vs TBK1 and 3.92 – 0 vs IKKe, imbuing several compounds with favorable properties relative to amlexanox (**5**) (LLE of 2.76 and 1.98, respectively). Utilizing cLogD_{7.4} in place of clogP in the equation[27] markedly enhances LLE for almost all compounds (calculations not shown). With regard to aqueous solubility, clogD_{7.4} values together with the number of aromatic rings in a given molecule provide a simple, useful guide of *potential* solubility of particular molecules with values ≤ 6 predicting for good aqueous solubility. Utilizing the SFI calculator, all compounds in Table SM2 are predicted to have acceptable aqueous solubility (SFI of 5.83 – 1.80) with many displaying lower SFI than amlexanox (3.32). These calculations correlate loosely with measured thermodynamic aqueous solubility values for selected compounds of Table SM2 (916 - <1.1 μM vs 172 μM for amlexanox). Measured solubility is highest for compounds with 2-propenyl (259 μM for **105**; 373 μM for **112**) and tetrazole (916 μM for **171**) substituents.

8. In vivo studies

Amlexanox (**5**) has been shown to reverse insulin resistance, inflammation, and hepatic steatosis in mice on a high fat diet.[29] Increased serum IL-6 levels are a robust biomarker of drug efficacy, and have been shown to be responsible for reducing fasting blood glucose levels in these mice and humans.[10],[25] Analogue **125**, which produced the most robust IL-6 production in 3T3-L1 cells, as well as a phosphorylation marker of efficacy, was investigated in obese mice and exhibited a serum IL-6 response similar to amlexanox (Figure 3A). Both amlexanox and **125** treatment resulted in a significant increase in serum IL-6 levels, but there was no significant difference between amlexanox and **125**. Further investigation of **125** showed a comparable weight loss effect over the course of 4 weeks (Figure 3B). After 4 weeks the body weight of amlexanox and **125** treated animals were both significantly lower than the vehicle controls, without any significant difference between the two treated groups. Intermediate glucose response (Figure 3C) and insulin sensitizing effect (Figure 3D) were observed in animals treated for 3–4 weeks. Analysis by one-way ANOVA revealed that all three groups were significantly different from each other in both the insulin and glucose tolerance tests. Overall, the effect of treatment with **125** closely resembles that of amlexanox, although with slightly altered kinetics.

9. Conclusions

As part of a research campaign to explore a new hypothesis on the role of inflammation in the generation of insulin resistance and type 2 diabetes, we have been focusing efforts on the design of small molecule inhibitors of TBK1 and IKK ϵ kinases, which are implicated as key mediators in insulin-independent pathways that promote energy storage and block adaptive energy expenditure during obesity. Toward that end, we are utilizing the clinically approved drug amlexanox (**5**), a modest inhibitor of TBK1 and IKK ϵ , as a starting point for analogue synthesis in order to develop an SAR that addresses some of its liabilities, principally modest potency and non-optimal aqueous solubility.

We previously reported the TBK1·amlexanox crystal structure, which revealed canonical ATP-competitive binding along the kinase hinge and demonstrated the importance of the carboxylic acid function for potent inhibition.[11] One of the goals of our work has been to improve on literature synthetic methodologies to make amlexanox analogues wherein A-ring substituents almost always had been incorporated early into a precursor 4-oxo-4*H*-1-benzopyran-3-carbonitrile. To introduce such substituents at a later stage and thus enhance overall route efficiency, we developed a novel palladium-catalyzed cross-coupling strategy on bromo precursors **6** – **10** to incorporate a range of R₇ and R₈ substituents. Due to the base sensitivity of key precursors using this strategy, it was necessary to devise a modified route to the C-6 isomer (**108**) of amlexanox.

Analogues with an olefinic substituent favor binding to IKK ϵ relative to saturated congeners, possibly due to the planarity of the sp² carbons (compare **105** vs **5**, **110** vs **109**, and **126** vs **125**). The presence of a serine residue at position 90 in the hinge of IKK ϵ , in contrast to a proline in TBK1, may affect the flexibility of the hinge region and, in conjunction with a planar olefinic moiety, allow for more kinase domain closure and improved binding. This trend is in line with prior SAR for the R₃ position of amlexanox,[11] but does not apply to 8-aza analogues (**112** vs **111**) wherein the isopropyl congener **111** shows a greater fold change in binding relative to amlexanox. For binding to 8-aza analogues, the hinge region may assume a conformation that allows for a hydrogen bond to form with the kinase backbone. This possibility is supported by the TBK1·amlexanox crystal structure wherein the hinge would need to change conformation in order for the 8-nitrogen to interact with the backbone.

Based on prior structural studies with amlexanox, cyclic R₇ modifications were predicted to extend through solvent and contact the neighboring dimerization domain. Docking experiments indicated the potential for global rearrangement of the inhibitor binding mode in such molecules. However, two independent co-crystal structures show that the inhibitor core of these analogues binds similarly to amlexanox along the hinge. R₇ cyclic substituents containing heteroatoms at the distal position (e.g., **149** and **150**) may interact with Tyr564, Lys570, or Lys576. More extended ring modifications such as acetylated piperidine (**146**) and spiroketal (**141**, **142**) may form contacts with the backbone of the dimerization domain.

The R₇ position tolerates ring sizes up to cyclohexyl after which potency markedly decreases, likely as a result of poor solubility and excessive bulk near the kinase hinge and P-loop. In line with the prior observation that inhibition of IKK ϵ is accentuated with olefinic

substituents attached to the R₇ position, analogue **126** retains inhibition of IKK ϵ while TBK1 inhibition is decreased. Appending saturated rings via short aliphatic linkers was detrimental to inhibition of both kinases due to poor solubility.

Some of the most striking results from our SAR campaign are shown by selected R₇ derivatives of Tables 1 and 2 that were further modified with the R₃ tetrazole, a carboxylic acid bioisostere. An analogue of amlexanox (**5**) bearing a tetrazole at the R₃ position was previously described to display a potency of 200–300 nM toward both TBK1 and IKK ϵ .^[11] When combined with a 6-membered hydrocarbon ring (**168**, **169**), dimethylamino (**170**), or morpholinyl (**171**) substituents, there were marginal changes in TBK1 potency relative to amlexanox. Unexpectedly, potency toward IKK ϵ was improved by nearly 25-fold (to 210 nM) compared to amlexanox for cyclohexenyl analogue **169**, suggesting that potency for IKK ϵ is optimized with a planar R₇ substituent near the hinge along with a R₃ tetrazole function. This potency is comparable to the R₃ tetrazole derivative of amlexanox suggesting that interactions with the gatekeeper Met86 and increased buried surface area drive potency even when a less favorable modification, such as a R₇ morpholine (**171**), is present. Thus, selectivity toward IKK ϵ for dual modified analogues may stem from increased hinge flexibility, allowing for the accommodation of two additional cyclic functions off the amlexanox pharmacophore. Conversely, the installation of an amide-linked tetrazole at the C-3 position was previously shown to decrease potency toward TBK1.^[11] However, when combined with a R₇ morpholinyl (**172**), potency is comparable to that of amlexanox.

In 3T3-L1 adipocytes, amlexanox (**5**) treatment promotes phosphorylation of TBK1 and p38, the latter of which induces beneficial IL-6 secretion. Movement of the isopropyl group to the C-6 position in **108** enhances p38 phosphorylation and downstream IL-6 secretion. Because the C-6 position of the pharmacophore projects toward the unoccupied P-loop, further SAR around this position may be more productive, despite a slight reduction in enzyme potency for **108** relative to amlexanox. Elongation of the isopropyl function to R₇ isobutyl (**116**) and isopentyl (**117**) greatly enhances IL-6 secretion and also enhances p38 or TBK1 phosphorylation. This result is surprising as both analogues display enzyme potencies comparable to amlexanox, even with a computed loss of solubility and lipophilic ligand efficiency (Table SM2). However, both inhibitors are predicted to have improved cellular permeability and may more readily enter cultured adipocytes. Analogue **148** bearing a R₇ unsaturated tetrahydropyran moiety elicited a similar IL-6 response despite the compound having a lower cLogP value. However, it is significantly more potent toward IKK ϵ , which may compensate for a lower permeability.

Most profound are the cellular effects by the R₇ cyclohexyl analogue **125**, which produced the greatest level of TBK1 phosphorylation and IL-6 secretion. Along with **117**, **125** is predicted to be highly cell permeable, which likely contributes to its efficacy. Interestingly, **125** is a poor enzyme inhibitor of IKK ϵ , displaying only minimal inhibition at 100 μ M. Thus, its cellular effects likely stem from inhibition of TBK1. When combined with a R₃ tetrazole moiety in **168**, the cellular response is abolished. In fact, all analogues bearing dual R₃ and R₇ modifications fail to elicit a cellular response. This observation is in line with a previous report that the introduction of an R₃ tetrazole without modification of the R₇ position eliminates cellular activity.^[11] The lack of cellular response may stem from

complex permeability effects that abrogate the beneficial effects of R₇ cyclohexyl incorporation.

In vivo experiments with **125** showed comparable efficacy to amlexanox (**5**) in obese mice. In contrast to robust secretion in cultured adipocytes, IL-6 production by **125** was only comparable *in vivo* to that of amlexanox (**5**). Similar effects on hepatic insulin response and glucose uptake were observed, although the **125** response lagged relative to amlexanox at some time points suggesting that the presence of a R₇ cyclohexyl moiety alters the kinetics of drug absorption and distribution. However, the endpoints for **125** were the same as amlexanox suggesting that the observed efficacy for these two inhibitors may be approaching a ceiling with respect to inhibition of TBK1 and IKK ϵ within the R₇ subclass of analogues.

In summary, future exploration of the amlexanox pharmacophore will be greatly aided by the synthetic methodology, co-crystal structure determinations, and SAR reported herein. Whereas several biomarkers in adipocytes of TBK1 and IKK ϵ are described, it remains to be seen whether the efficacy of amlexanox or **125** represents the maximum response that can be achieved through inhibition of these targets. As the C-6 isomer of amlexanox displayed improved cellular response, the installation of additional modifications at this position presents an attractive direction toward enhancing enzyme potency through burying surface area under the P-loop. That along with careful consideration of physicochemical properties, such as permeability and solubility, will aid in the identification of inhibitors that might produce a more efficacious response *in vivo*. Further SAR exploration of the amlexanox pharmacophore, as well as truncated core congeners, is ongoing and will reveal whether these efforts lead to clinical candidates for the treatment of type 2 diabetes and/or obesity.

10. Experimental

Chemistry. *Materials and Methods.*

All starting monomers were obtained from commercial suppliers and were used without further purification. Amlexanox, >99% pure by HPLC, was purchased from Ontario Chemicals, Inc. 2-Amino-7-bromo-5-oxo-5*H*-[1]benzopyrano[2,3-*b*]pyridine-3-carbonitrile was purchased from Sigma-Aldrich. Routine ¹H NMR spectra were recorded at 400 or 500 MHz on a Varian 400 or 500 instrument, respectively, with CDCl₃ or DMSO-*d*₆ as solvent. Chemical shift values are recorded in δ units (ppm). Mass spectra were recorded on a Micromass ToFSpec-2E Matrix-Assisted, Laser-Desorption, Time-of-Flight Mass Spectrometer in a positive ESI mode (TOFES⁺) unless otherwise noted. High resolution mass spectrometry (HRMS) analysis was performed on an Agilent Q-TOF system. Analytical HPLC was performed on an Agilent 1100 series instrument with an Agilent Zorbax Eclipse Plus C18 (4.6 mm \times 75 mm, 3.5 μ m particle size) column with the gradient 10% acetonitrile/water (1 min), 10–90% acetonitrile/water (6 min), and 90% acetonitrile/water (2 min) flow = 1 mL/min. Thin-layer chromatography (TLC) was performed on silica gel GHLF plates (250 μ m) purchased from Analtech. Column chromatography was carried out in the flash mode utilizing silica gel (220–240 mesh) purchased from Silicycle. Extraction solutions were dried over anhydrous sodium sulfate prior to concentration.

Method A: Palladium-catalyzed cross coupling reactions**(a) Suzuki couplings[17]**

1.1 1-(2-Hydroxy-6-(prop-1-en-2-yl)phenyl)ethan-1-one (92; Scheme 3).: A solution of nitrogen-degassed potassium carbonate (964 mg, 6.98 mmol) in water (1.2 mL) was added to a nitrogen-degassed mixture of compound **85** (500 mg, 2.33 mmol), triphenylphosphine (18.3 mg, 0.070 mmol), potassium trifluoro(prop-1-en-2-yl)borate, (475 mg, 3.21 mmol), and PdCl₂(PPh₃)₂ (16.3 mg, 0.023 mmol) in tetrahydrofuran (3.6 mL). The reaction vial was sealed and heated at 100 °C for 18 h. The mixture was cooled to room temperature and diluted with saturated aqueous ammonium chloride and then extracted with dichloromethane (3x) and. The combined organic phases were washed by brine, dried, and concentrated to give **92** (0.40 g, 98%) as an orange oil. ¹H NMR (500 MHz, chloroform-*d*): δ 11.48 (s, 1H), 7.32 (ddd, *J* = 8.2, 7.5, 0.6 Hz, 1H), 6.89 (ddd, *J* = 8.4, 1.3, 0.6 Hz, 1H), 6.76 (ddd, *J* = 7.5, 1.2, 0.6 Hz, 1H), 5.24 (dt, *J* = 2.0, 1.0 Hz, 1H), 4.97 (dt, *J* = 1.7, 0.9 Hz, 1H), 2.57 (d, *J* = 0.6 Hz, 3H), 2.17 (dt, *J* = 1.5, 0.7 Hz, 3H). MS: *m/z* 177.0908 (M+H)⁺.

1.2 2-Amino-7-(cyclohex-1-en-1-yl)-5-oxo-5H-chromeno[2,3-b]pyridine-3-carbonitrile (102; Scheme 4).: A solution of tripotassium phosphate (701 mg, 3.3 mmol) in water (1.5 mL) was added to a nitrogen-degassed suspension of 2-amino-7-bromo-5-oxo-5H-chromeno[2,3-*b*]pyridine-3-carbonitrile (**101**; 174 mg, 0.55 mmol), 2-(cyclohex-1-en-1-yl)-4,4,5,5-tetramethyl-1,3,2-dioxaborolane (252 mg, 1.21 mmol), triphenylphosphine (72.2 mg, 0.28 mmol), and Pd(OAc)₂ (12.4 mg, 0.06 mmol) in *p*-dioxane (13 mL). The reaction vessel was sealed with a screw cap and heated at 100–110 °C for 30 min and then stirred at 70 °C for 1.5 h. After cooling, the mixture was concentrated and the residue was diluted with a mixture of water and dichloromethane. Precipitated solids were collected and the organic phase of the biphasic filtrate was dried and concentrated to leave additional solids. The combined solids were triturated in dichloromethane and dried to give **102** (136 mg, 78%) as an orange solid. ¹H NMR (400 MHz, DMSO-*d*₆): δ 8.61 (s, 1H), 8.13 (s, 2H), 7.97 (d, *J* = 2.3 Hz, 1H), 7.89 (dd, *J* = 8.8, 2.4 Hz, 1H), 7.52 (d, *J* = 8.7 Hz, 1H), 6.29 (s, 1H), 2.41 (s, 2H), 2.21 (s, 2H), 1.82–1.70 (m, 2H), 1.62 (t, *J* = 5.8 Hz, 2H). MS: *m/z* 318.0 (M+H)⁺.

See Supplementary Material for additional experimental procedures: **15-18, 24** (Scheme SM1); **32, 36-52, 55-58** (Scheme SM2)

(b) Sonogashira coupling[18]

1.1 Ethyl 2-amino-7-(3-methylbut-1-yn-1-yl)-5-oxo-5H-chromeno[2,3-b]pyridine-3-carboxylate (19; Scheme SM1).: A suspension of compound **9** (300 mg, 0.83 mmol), 3-methylbut-1-yne (338 mg, 4.96 mmol), triphenylphosphine (21.7 mg, 0.08 mmol), *N,N*-dimethylformamide (8 mL), tetrahydrofuran (8 mL), and triethylamine (7.5 mL) in a 100 mL sealed tube was degassed with nitrogen. Then Pd(PPh₃)₄ (47.7 mg, 0.04 mmol) and CuI (15.7 mg, 0.08 mmol) were added under an atmosphere of nitrogen and the suspension was heated at 85 °C for 18 h. The mixture was diluted with water and extracted with dichloromethane (2x). The organic phases were dried and concentrated to leave a solid that was triturated in ethanol and then diethyl ether, and dried to give **19** (246 mg, 85%) as a solid. ¹H NMR (400 MHz, chloroform-*d*) δ 9.14 (s, 1H), 8.38 (s, 1H), 8.28 (d, *J* = 2.1 Hz,

1H), 7.69 (dd, $J = 8.6, 2.1$ Hz, 1H), 7.41 (d, $J = 8.6$ Hz, 1H), 5.92 (s, 1H), 4.40 (q, $J = 7.1$ Hz, 2H), 2.80 (p, $J = 6.9$ Hz, 1H), 1.43 (dd, $J = 7.6, 6.7$ Hz, 3H), 1.29 (dd, $J = 7.0, 1.0$ Hz, 6H). MS m/z 351.1341 (M+1)⁺.

1.2 Ethyl 2-amino-8-fluoro-7-(3-methylbut-1-yn-1-yl)-5-oxo-5H-chromeno[2,3-b]pyridine-3-carboxylate (20; Scheme SM1).: Similar reaction of **7** (40 mg, 0.11 mmol), 3-methylbut-1-yne (43 mg, 0.63 mmol), triphenylphosphine (2.8 mg, 10.5 μ mol), Pd(PPh₃)₄ (6.1 mg, 5.3 μ mol), CuI (2.0 mg, 10.5 μ mol), triethylamine (2 mL), *N,N*-dimethylformamide (2 mL), and tetrahydrofuran (2 mL) gave **20** (26 mg, 67%) as a solid. ¹H NMR (500 MHz, chloroform-*d*) δ 9.12 (s, 1H), 8.40 (s, 1H), 8.32 (d, $J = 7.8$ Hz, 1H), 7.17 (d, $J = 9.2$ Hz, 1H), 5.89 (s, 1H), 4.40 (q, $J = 7.1$ Hz, 2H), 2.83 (q, $J = 6.9$ Hz, 1H), 1.43 (t, $J = 7.2$ Hz, 3H), 1.35 – 1.26 (m, 6H). MS m/z 369.12 (M+1)⁺.

1.3 Ethyl 2-amino-7-(3-(dimethylamino)prop-1-yn-1-yl)-5-oxo-5H-chromeno[2,3-b]pyridine-3-carboxylate (21; Scheme SM1).: Similar reaction of **9** (400 mg, 1.10 mmol), 3-dimethylamino-1-propyne (275 mg, 3.3 mmol), CuI (42 mg, 0.22 mmol), (Ph₃P)₂PdCl₂ (77 mg, 0.11 mmol), triethylamine (20 mL), and *N,N*-dimethylformamide (6 mL) at 80 °C overnight gave a residue that was purified by flash silica gel chromatography, eluting with 3% methanol in dichloromethane, to provide **21** (320 mg, 80%) as light orange solid following sonication in methanol. ¹H NMR (400 MHz, chloroform-*d*) δ 9.15 (s, 1H), 8.40 (s, 1H), 8.33 (d, $J = 2.0$ Hz, 1H), 7.82 – 7.68 (m, 1H), 7.44 (d, $J = 8.6$ Hz, 1H), 5.88 (s, 1H), 4.49 – 4.33 (m, 2H), 3.50 (s, 2H), 2.39 (s, 6H), 1.44 (td, $J = 7.1, 1.1$ Hz, 3H). MS m/z 366.0 (M+H)⁺.

1.1 Ethyl 2-amino-7-(cyclopropylethynyl)-5-oxo-5H-chromeno[2,3-b]pyridine-3-carboxylate (53; Scheme SM2).: Similar reaction of **9** (500 mg, 1.38 mmol), ethynylcyclopropane (364 mg, 5.51 mmol), triphenylphosphine (36.1 mg, 0.14 mmol), *N,N*-dimethylformamide (10 mL), tetrahydrofuran (10 mL), triethylamine (10 mL), Pd(PPh₃)₄ (80 mg, 0.07 mmol) and CuI (26.2 mg, 0.14 mmol) gave **53** (452 mg, 94%) as solid. ¹H NMR (400 MHz, chloroform-*d*) δ 9.14 (s, 1H), 8.39 (s, 1H), 8.26 (s, 1H), 7.67 (dd, $J = 8.5, 2.1$ Hz, 1H), 7.40 (d, $J = 8.6$ Hz, 1H), 5.91 (s, 1H), 4.40 (q, $J = 7.1$ Hz, 2H), 1.52 – 1.46 (m, 1H), 1.43 (t, $J = 7.2$ Hz, 3H), 0.90 (d, $J = 8.1$ Hz, 2H), 0.88 – 0.80 (m, 2H). MS m/z 349.12 (M+1)⁺.

2. Ethyl 2-amino-7-(cyclobutylethynyl)-5-oxo-5H-chromeno[2,3-b]pyridine-3-carboxylate (54; Scheme SM2).: Similar reaction of **9** (200 mg, 0.55 mmol), triphenylphosphine (14.4 mg, 0.06 mmol), *N,N*-dimethylformamide (4 mL), tetrahydrofuran (4 mL), triethylamine (4 mL), ethynylcyclopropane[30] (220 mg, 2.75 mmol), Pd(PPh₃)₄ (31.7 mg, 0.03 mmol) and CuI (10.5 mg, 0.06 mmol) gave **54** (173 mg, 87%) as a solid. The compound was used directly in the next step.

(c) Negishi coupling[19]

2.1 Ethyl 2-((tert-butoxycarbonyl)amino)-7-isobutyl-5-oxo-5H-chromeno[2,3-b]pyridine-3-carboxylate (22; Scheme SM1).: A mixture of isobutylzinc(II) bromide solution (7.5 ml, 0.5 M in tetrahydrofuran, 3.75 mmol), compound **10** (300 mg, 0.65 mmol)

and PdCl₂(dppf) · CH₂Cl₂ (53 mg, 0.07 mmol) was degassed with nitrogen and the reaction vial capped. The mixture was heated at 67 °C for 16 h, cooled, diluted with water, and extracted with dichloromethane (2x). The combined organic phases were washed with saturated aq NaHCO₃ and then brine, dried, and concentrated to leave a solid that was purified by silica gel preparative plate chromatography (elution with 0.2% methanol in dichloromethane) to afford **22** (72 mg, 25%). ¹H NMR (400 MHz, chloroform-*d*) δ 10.89 (s, 1H), 9.29 (d, *J* = 0.8 Hz, 1H), 8.04 (dd, *J* = 1.8, 0.9 Hz, 1H), 7.54 (t, *J* = 1.3 Hz, 2H), 4.46 (q, *J* = 7.1 Hz, 2H), 2.61 (d, *J* = 7.2 Hz, 2H), 1.94 (dt, *J* = 13.6, 6.8 Hz, 1H), 1.58 (s, 9H), 1.47 (t, *J* = 7.2 Hz, 3H), 0.94 (d, *J* = 6.6 Hz, 6H). MS *m/z* 441.2032 (M+H)⁺.

2.2 Ethyl 2-((tert-butoxycarbonyl)amino)-7-cyclobutyl-5-oxo-5H-chromeno[2,3-*b*]pyridine-3-carboxylate (34; Scheme SM2).: Similar reaction of **10** (200 mg, 0.43 mmol), cyclobutylzinc(II) bromide (5.0 ml of 0.5 M solution in tetrahydrofuran, 2.5 mmol), Pd(dppf)Cl₂ · CH₂Cl₂ (35.3 mg, 0.04 mmol) gave **34** (50 mg, 26%). ¹H NMR (400 MHz, chloroform-*d*): δ 10.89 (s, 1H), 9.30 (d, *J* = 0.9 Hz, 1H), 8.10 (d, *J* = 2.3 Hz, 1H), 7.68 – 7.57 (m, 1H), 7.54 (d, *J* = 8.6 Hz, 1H), 4.47 (q, *J* = 7.1 Hz, 2H), 3.66 (t, *J* = 8.9 Hz, 1H), 2.42 (dtd, *J* = 10.4, 7.9, 2.4 Hz, 2H), 2.27 – 2.14 (m, 2H), 2.14 – 1.98 (m, 1H), 1.95 – 1.84 (m, 1H), 1.58 (s, 9H), 1.47 (t, *J* = 7.1 Hz, 3H). MS TOFES⁺: *m/z* 439.1 (M+H)⁺.

(d) Stille coupling[20]

2.3 4-Oxo-5-(prop-1-en-2-yl)-4H-chromene-3-carbonitrile (89; Scheme 3).: A mixture of compound **88** (1.0 g, 4.0 mmol), tri-*n*-butyl(prop-1-en-2-yl)stannane (1.46 g, 4.4 mmol), and Pd(PPh₃)₂Cl₂ (281 mg, 0.4 mmol) in a vial was flushed with nitrogen. Dry *p*-dioxane (20 mL) was added and the mixture was degassed and flushed with nitrogen. This vial was sealed and heated at 100 °C for 20 min and then at 80 °C for 16 h after which the mixture was diluted with water and extracted with dichloromethane. The organic phase was dried and concentrated to leave a residue that was purified by preparative plate silica gel chromatography (25–50% ethyl acetate in hexanes) to give **89** (680 mg, 81%) as a solid. ¹H NMR (400 MHz, chloroform-*d*): δ 8.36 (s, 1H), 7.69 (dd, *J* = 8.5, 7.4 Hz, 1H), 7.47 (dd, *J* = 8.5, 1.2 Hz, 1H), 7.24 (dd, *J* = 7.4, 1.2 Hz, 1H), 5.18 (t, *J* = 1.6 Hz, 1H), 4.89 – 4.78 (m, 1H), 2.09 (t, *J* = 1.1 Hz, 3H). MS: *m/z* 212.0702 (M+H)⁺.

(e) Buchwald coupling[21]

2.4 1-(5-(Dimethylamino)-2-hydroxyphenyl)ethan-1-one (97a; Scheme 4).: To a nitrogen-degassed solution of **96** (3.0 g, 13.95 mmol) was added dimethylamine (27.9 ml, 2M in tetrahydrofuran, 55.8 mmol), lithium hexamethyldisilazide (48.8 mL, 1M in tetrahydrofuran, 48.8 mmol), Pd₂(dba)₃ (204 mg, 0.223 mmol), and 2-dicyclohexylphosphino-2'-*N,N*-(dimethylamino)biphenyl (DavePhos; 176 mg, 0.446 mmol). The mixture was degassed again with nitrogen, sealed in a capped vial and stirred at 80 °C for 2 h. After cooling, the mixture was concentrated to a residue that was distributed between dichloromethane and saturated aqueous ammonium chloride solution. The organic phase was washed with brine and concentrated to give crude **97a** (2.5 g, 100%) as a solid. ¹H NMR (400 MHz, chloroform-*d*) δ 11.74 (s, 1H), 7.08 (dd, *J* = 9.0, 3.1 Hz, 1H), 7.01 (d, *J* = 3.0 Hz, 1H), 6.91 (d, *J* = 9.0 Hz, 1H), 2.89 (d, *J* = 1.1 Hz, 6H), 2.62 (d, *J* = 1.1 Hz, 3H). MS *m/z* 180.1 (M+H)⁺.

2.5 1-(2-Hydroxy-5-morpholinophenyl)ethan-1-one (97b; Scheme 4).: Reaction of **96** (2.0 g, 9.3 mmol) in tetrahydrofuran (15 mL), morpholine (1.3 g, 14.9 mmol), lithium hexamethyldisilazide (32.6 mL, 1 M in tetrahydrofuran, 32.6 mmol), Pd₂(dba)₃ (136 mg, 0.15 mmol), and 2-dicyclohexylphosphino-2'-N,N-(dimethylamino)biphenyl (DavePhos; 117 mg, 0.30 mmol) at 75 °C for 1 h, as described above for the synthesis of **97a**, gave an oil that was purified by flash silica gel chromatography, eluting with 0.5:1:100 trimethylamine solution (25% w/w solution in methanol) : methanol : dichloromethane to give **97b** (1.67 g, 81%) as a solid. ¹H NMR (400 MHz, chloroform-*d*): δ 11.92 (s, 1H), 7.22 – 7.18 (m, 2H), 6.97 – 6.92 (m, 1H), 3.93 – 3.82 (m, 4H), 3.10 – 3.01 (m, 4H), 2.63 (s, 3H). MS TOFES⁺: *m/z* 222.1 (M+H)⁺.

Method B: Formation of Boc derivatives of ethyl 2-amino-5-oxo-5H-chromeno[2,3-*b*]pyridine-3-carboxylates[31]

2.6 Ethyl 7-bromo-2-((tert-butoxycarbonyl)amino)-5-oxo-5H-chromeno[2,3-*b*]pyridine-3-carboxylate (10; Scheme SM1).: To a suspension of compound **9** (50 mg, 0.14 mmol, and 4-dimethylaminopyridine (1 mg, 8.2 μmol) in dichloromethane (5 mL) was added di-*tert*-butyl dicarbonate (33 mg, 0.15 mmol) portion-wise. The mixture was stirred at room temperature for 16 h. The solid was collected by filtration, washed with dichloromethane (2 mL) and dried to afford **10** (53 mg, 83%) as a white solid. ¹H NMR (400 MHz, chloroform-*d*): δ 10.91 (s, 1H), 9.28 (d, *J* = 0.9 Hz, 1H), 8.41 (d, *J* = 2.4 Hz, 1H), 7.83 (dd, *J* = 8.9, 2.5 Hz, 1H), 7.51 (d, *J* = 8.9 Hz, 1H), 4.46 (q, *J* = 7.1 Hz, 2H), 1.58 (d, *J* = 0.9 Hz, 9H), 1.47 (t, *J* = 7.1 Hz, 3H). MS TOFES⁻: *m/z* 460.9, 462.9 (M-H)⁻.

Method C: TFA deprotection of ethyl 2-((tert-butoxycarbonyl)amino)-5-oxo-5H-chromeno[2,3-*b*]pyridine-3-carboxylates[32]

2.7 Ethyl 2-amino-7-isobutyl-5-oxo-5H-chromeno[2,3-*b*]pyridine-3-carboxylate (23; Scheme SM1).: To a solution of compound **22** (71 mg, 0.16 mmol) in dichloromethane (10 mL) was added trifluoroacetic acid (0.25 mL) and the mixture was stirred for 15 min at room temperature. The mixture was washed with saturated aq NaHCO₃, dried, and concentrated to give **23** (53 mg, 97%) as a solid. ¹H NMR (400 MHz, chloroform-*d*) δ 9.15 (s, 1H), 8.36 (s, 1H), 8.03 (d, *J* = 2.1 Hz, 1H), 7.54 – 7.49 (m, 1H), 7.42 (d, *J* = 8.5 Hz, 1H), 5.93 (s, 1H), 4.41 (q, *J* = 7.1 Hz, 2H), 2.60 (d, *J* = 7.2 Hz, 2H), 1.93 (dt, *J* = 13.5, 6.8 Hz, 1H), 1.44 (t, *J* = 7.1 Hz, 3H), 0.93 (d, *J* = 6.6 Hz, 6H). MS *m/z* 341.1522 (M+H)⁺.

2.8 Ethyl 2-amino-7-cyclopropyl-5-oxo-5H-chromeno[2,3-*b*]pyridine-3-carboxylate (33; Scheme SM2).: Similar reaction of **32** (59 mg, 0.14 mmol), trifluoroacetic acid (0.5 mL), and dichloromethane (20 mL) gave **33** (45 mg, 100%) as a white solid. ¹H NMR (400 MHz, DMSO-*d*₆): δ 8.80 (s, 1H), 8.34 (s, 1H), 8.09 (s, 1H), 7.77 (d, *J* = 2.2 Hz, 1H), 7.58 – 7.42 (m, 2H), 4.35 (q, *J* = 7.1 Hz, 2H), 2.11 (dt, *J* = 8.5, 3.7 Hz, 1H), 1.36 (t, *J* = 7.1 Hz, 3H), 1.07 – 0.92 (m, 2H), 0.79 – 0.65 (m, 2H). MS TOFES⁺: *m/z* 325.0 (M+H)⁺.

2.9 Ethyl 2-amino-7-cyclobutyl-5-oxo-5H-chromeno[2,3-*b*]pyridine-3-carboxylate (35; Scheme SM2).: Similar reaction of **34** (50 mg, 0.11 mmol), trifluoroacetic acid (0.5 mL), and dichloromethane (20 mL) for 1 h gave **35** (39 mg, 100%) as a white solid. ¹H NMR (400 MHz, chloroform-*d*): δ 9.15 (s, 1H), 8.36 (s, 1H), 8.09 (d, *J* = 2.2 Hz, 1H), 7.56 (ddd, *J* =

8.5, 2.3, 0.7 Hz, 1H), 7.43 (d, $J = 8.5$ Hz, 1H), 5.91 (s, 1H), 4.41 (q, $J = 7.1$ Hz, 2H), 3.65 (p, $J = 8.8$ Hz, 1H), 2.41 (dtd, $J = 10.5, 8.0, 2.4$ Hz, 2H), 2.21 (pd, $J = 9.6, 2.0$ Hz, 2H), 2.12 – 2.01 (m, 1H), 1.95 – 1.82 (m, 1H), 1.44 (t, $J = 7.1$ Hz, 3H). MS TOFES⁺: m/z 339.1 (M+H)⁺.

2.10 Ethyl 2-amino-7-cycloheptyl-5-oxo-5H-chromeno[2,3-b]pyridine-3-carboxylate (62; Scheme SM2): Similar reaction of **61** (105 mg, 0.23 mmol), trifluoroacetic acid (0.5 mL) and dichloromethane (20 mL) for 30 min gave **62** (82 mg, 94%) as a solid. ¹H NMR (400 MHz, chloroform-*d*): δ 9.15 (s, 1H), 8.35 (s, 1H), 8.06 (d, $J = 2.3$ Hz, 1H), 7.55 (dd, $J = 8.6, 2.3$ Hz, 1H), 7.41 (d, $J = 8.6$ Hz, 1H), 5.88 (s, 1H), 4.40 (q, $J = 7.2$ Hz, 2H), 2.87 – 2.74 (m, 1H), 1.97 – 1.88 (m, 2H), 1.82 (dt, $J = 9.5, 3.3$ Hz, 2H), 1.72 (td, $J = 10.3, 3.4$ Hz, 4H), 1.61 (d, $J = 6.5$ Hz, 4H), 1.44 (t, $J = 7.1$ Hz, 3H). MS TOFES⁺: m/z 381.1 (M+H)⁺.

2.11 Ethyl 2-amino-5-oxo-7-(piperidin-4-yl)-5H-chromeno[2,3-b]pyridine-3-carboxylate, trifluoroacetic acid salt (71; Scheme SM2): Similar reaction of **70** (100 mg, 0.21 mmol), trifluoroacetic acid (0.25 mL), and dichloromethane (10 mL) for 5 h at 40 °C, but without the extractive workup, gave crude **71** (115 mg, 100%) as an off-white solid. It was used directly in the next step. ¹H NMR (400 MHz, chloroform-*d*): δ 9.17 (s, 1H), 8.70 (s, 1H), 8.62 (s, 1H), 8.20 (s, 1H), 8.13 (d, $J = 2.2$ Hz, 1H), 7.63 (d, $J = 2.3$ Hz, 1H), 7.55 (s, 1H), 4.42 (q, $J = 7.1$ Hz, 2H), 3.70 (d, $J = 12.7$ Hz, 2H), 3.18 (d, $J = 12.0$ Hz, 2H), 3.00 (d, $J = 10.9$ Hz, 1H), 2.15 (d, $J = 22.9$ Hz, 4H), 1.44 (t, $J = 7.1$ Hz, 3H). MS TOFES⁺: m/z 368.1 (M+H)⁺.

Method D: Hydrogenation of olefins/alkynes to alkyl derivatives[33]

2.12 Ethyl 2-amino-6-isopropyl-5-oxo-5H-chromeno[2,3-b]pyridine-3-carboxylate (91; Scheme 3): A flask with a solution of compound **90** (500 mg, 1.54 mmol) in dichloromethane (50 mL) and ethanol (100 mL) was purged with nitrogen and 10% palladium on carbon (400 mg) was added. The mixture was purged with nitrogen and hydrogen, and hydrogenated at 45 psi using a Parr shaker at room temperature for 45 h. The mixture was filtered over Celite[®] and concentrated to a solid that triturated in ethanol and dried to give **91** (392 mg, 78%) as a white solid. ¹H NMR (400 MHz, chloroform-*d*): δ 9.12 (s, 1H), 8.32 (s, 1H), 7.61 (t, $J = 8.0$ Hz, 1H), 7.36 (ddd, $J = 15.2, 8.0, 1.2$ Hz, 2H), 6.00 (s, 1H), 4.75 (p, $J = 6.8$ Hz, 1H), 4.38 (q, $J = 7.1$ Hz, 2H), 1.42 (t, $J = 7.1$ Hz, 3H), 1.32 (d, $J = 6.8$ Hz, 6H). MS: m/z 327.1341 (M+H)⁺.

2.13 1-(2-Hydroxy-6-isopropylphenyl)ethan-1-one (94; Scheme 3): Made similarly as **91** from compound **92** (370 mg, 2.1 mmol) in dichloromethane (10 mL) and ethanol (20 mL) over 10% palladium on carbon (220 mg) at atmospheric pressure of hydrogen for 18 h. Workup left **94** (357 mg, 95%) as a gum. ¹H NMR (400 MHz, chloroform-*d*) δ 7.21 (t, $J = 8.0$ Hz, 1H), 6.86 (dd, $J = 7.8, 1.0$ Hz, 1H), 6.72 (dd, $J = 8.1, 1.1$ Hz, 1H), 3.71 (q, $J = 7.0$ Hz, 1H), 3.08 (p, $J = 6.8$ Hz, 1H), 2.59 (d, $J = 0.8$ Hz, 3H), 1.24 (d, $J = 6.8$ Hz, 6H). MS: m/z 179.1061 (M+H)⁺.

2.14 2-Amino-7-cyclohexyl-5-oxo-5H-chromeno[2,3-b]pyridine-3-carbonitrile (103; Scheme 4): Made similarly as **91** from compound **102** (58 mg, 0.18 mmol) in

dichloromethane (90 mL) and ethanol (80 mL) over 10% palladium on carbon (80 mg) at 42 psi of hydrogen for 22 h. Workup gave **103** (44 mg, 75%) as a white solid. $^1\text{H NMR}$ (500 MHz, chloroform-*d*): δ 8.75 (s, 1H), 8.08 (d, $J = 2.3$ Hz, 1H), 7.60 (dd, $J = 8.6, 2.3$ Hz, 1H), 7.44 (d, $J = 8.6$ Hz, 1H), 5.76 (s, 2H), 2.63 (d, $J = 3.4$ Hz, 1H), 1.90 (dd, $J = 19.2, 12.5$ Hz, 4H), 1.78 (d, $J = 13.2$ Hz, 1H), 1.52 – 1.36 (m, 4H), 1.29 (m, 1H). MS TOFES⁺: m/z 320.0 (M+H)⁺.

See Supplementary Material for additional experimental procedures: **25-31** (Scheme SM1); **59-61, 63-70, 74, 75, 77-84** (Scheme SM2)

Method E: Base hydrolysis of ethyl esters to carboxylic acids[34]

1.1 2-Amino-6-isopropyl-5-oxo-5H-chromeno[2,3-*b*]pyridine-3-carboxylic acid (108; Scheme 3): To a suspension of **91** (380 mg, 1.2 mmol) in ethanol (50 mL) and water (6.25 mL) was added 1 N aq NaOH (6.25 mL). The mixture was stirred for 1.5 h at 50 °C and filtered. The filtrate was concentrated to a solid that was suspended in water (50 mL) and acidified with 1N aq. HCl to pH 3–4. The precipitated solids were stirred at room temperature for 24 h, collected, washed with water, and dried to give **108** (298 mg, 86%). HPLC: rt 6.6 min (98% purity) (98%). $^1\text{H NMR}$ (400 MHz, DMSO-*d*₆): δ 13.40 (s, 1H), 8.78 (s, 1H), 8.21 (s, 2H), 7.72 (t, $J = 8.0$ Hz, 1H), 7.48 – 7.37 (m, 2H), 4.71 (p, $J = 6.8$ Hz, 1H), 1.24 (d, $J = 6.8$ Hz, 6H). MS: m/z 299.1026 (M+H)⁺.

1.2 2-Amino-7-(dimethylamino)-5-oxo-5H-chromeno[2,3-*b*]pyridine-3-carboxylic acid (113; Scheme 4): Made similarly from **100a** to give **113** (83 mg, 91%). HPLC: rt 4.1 min (93% purity) $^1\text{H NMR}$ (400 MHz, DMSO-*d*₆) δ 13.41 (s, 1H), 8.79 (s, 1H), 8.19 (s, 2H), 7.46 (d, $J = 9.1$ Hz, 1H), 7.29 (dd, $J = 9.2, 3.2$ Hz, 1H), 7.17 (d, $J = 3.1$ Hz, 1H), 2.97 (s, 6H). MS m/z 300.0 (M+H)⁺.

1.1 2-Amino-7-morpholino-5-oxo-5H-chromeno[2,3-*b*]pyridine-3-carboxylic acid (151; Scheme 4): Made similarly from **100b** to give **151** (180 mg, 85%). HPLC: rt 5.2 min (94% purity). $^1\text{H NMR}$ (400 MHz, DMSO-*d*₆): δ 13.44 (s, 1H), 8.80 (d, $J = 3.8$ Hz, 1H), 8.22 (s, 2H), 7.60 – 7.47 (m, 2H), 7.41 (d, $J = 3.3$ Hz, 1H), 3.77 (t, $J = 4.7$ Hz, 4H), 3.18 (d, $J = 5.1$ Hz, 4H). MS TOFES⁺: m/z 342.0 (M+H)⁺.

See Supplementary Material for additional experimental procedures: **105-107, 109-112, 114-121** (Scheme SM1); **122-139, 141-150, 152-167** (Scheme SM2)

Method F: N-acylations

1.2 Ethyl 2-amino-7-(1-formylpiperidin-4-yl)-5-oxo-5H-chromeno[2,3-*b*]pyridine-3-carboxylate (72; Scheme SM2): A solution of compound **71** (103 mg, 0.21 mmol), triethylamine (0.21 ml, 1.5 mmol), formic acetic anhydride (28.3 mg, 0.32 mmol) and dichloromethane (25 mL) was stirred at room temperature for 10 min and concentrated to a white solid that was triturated in diethyl ether and dried to give **72** (66 mg, 78%). $^1\text{H NMR}$ (400 MHz, chloroform-*d*): δ 9.16 (d, $J = 2.1$ Hz, 1H), 8.39 (s, 1H), 8.10 (q, $J = 2.4$ Hz, 2H), 7.56 (d, $J = 8.5$ Hz, 1H), 7.47 (dd, $J = 8.6, 2.3$ Hz, 1H), 5.91 (s, 1H), 4.62 (d, $J = 13.5$ Hz, 1H), 4.47 – 4.34 (m, 2H), 3.79 (d, $J = 13.6$ Hz, 1H), 3.25 (t, $J = 13.3$ Hz, 1H), 2.94 (t, $J =$

12.7 Hz, 1H), 2.76 (t, $J = 13.0$ Hz, 1H), 2.04 – 1.91 (m, 2H), 1.69 (dd, $J = 16.7, 10.8$ Hz, 2H), 1.44 (td, $J = 7.2, 2.2$ Hz, 3H). MS TOFES⁺: m/z 396.1 (M+H)⁺.

1.3 Ethyl 7-(1-acetylpiperidin-4-yl)-2-amino-5-oxo-5H-chromeno[2,3-b]pyridine-3-carboxylate (73; Scheme SM2): Reaction of **71** (103 mg, 0.21 mmol) with acetic anhydride (33 mg, 0.32 mmol) gave crude **73** (quantitative) that was used directly in the next step. ¹H NMR (500 MHz, chloroform-*d*): δ 9.15 (d, $J = 1.5$ Hz, 1H), 8.37 (s, 1H), 8.09 (t, $J = 1.8$ Hz, 1H), 7.56 (dt, $J = 8.6, 1.9$ Hz, 1H), 7.46 (dd, $J = 8.6, 1.4$ Hz, 1H), 6.00 (s, 1H), 4.87 – 4.76 (m, 1H), 4.41 (qd, $J = 7.1, 1.5$ Hz, 2H), 4.04 – 3.92 (m, 1H), 3.24 – 3.18 (m, 1H), 2.93 – 2.84 (m, 1H), 2.66 (dd, $J = 14.2, 11.5$ Hz, 1H), 2.16 (d, $J = 1.4$ Hz, 3H), 2.01 – 1.88 (m, 2H), 1.70 (ddd, $J = 24.7, 12.3, 4.3$ Hz, 2H), 1.44 (td, $J = 7.1, 1.5$ Hz, 3H). MS TOFES⁺: m/z 410.1 (M+H)⁺.

Method G: Sulfone oxidation

1.4 Ethyl 2-amino-7-(1,1-dioxidotetrahydro-2H-thiopyran-4-yl)-5-oxo-5H-chromeno[2,3-b]pyridine-3-carboxylate (76; Scheme SM2): An ice-cold solution of compound **75** (55 mg, 0.14 mmol) in dichloromethane (10 mL) was treated portion-wise with 3-chlorobenzoperoxoic acid (106 mg of 70% purity, 0.43 mmol) and the mixture was stirred for 30 min at room temperature. The mixture was washed successively with 5% aq. Na₂CO₃, water, and brine, dried, and purified by silica gel preparative plate chromatography (elution with 3.5% methanol in dichloromethane) to give **76** (33 mg, 55%) as a solid. ¹H NMR (400 MHz, chloroform-*d*): δ 9.16 (s, 1H), 8.41 (s, 1H), 8.14 (d, $J = 2.3$ Hz, 1H), 7.60 (dd, $J = 8.6, 2.4$ Hz, 1H), 7.49 (d, $J = 8.6$ Hz, 1H), 5.91 (s, 1H), 4.41 (q, $J = 7.1$ Hz, 2H), 3.19 (dd, $J = 8.8, 3.3$ Hz, 4H), 2.96 (t, $J = 12.3$ Hz, 1H), 2.49 (dt, $J = 13.7, 6.1$ Hz, 2H), 2.28 (d, $J = 14.4$ Hz, 2H), 1.44 (t, $J = 7.1$ Hz, 3H). MS: m/z 417.0 (M+H)⁺.

Method H: Ketal hydrolysis

1.5 2-Amino-5-oxo-7-(4-oxocyclohexyl)-5H-chromeno[2,3-b]pyridine-3-carboxylic acid (140; Scheme SM2): A suspension of compound **141** (29 mg, 0.07 mmol) in 7.5N aqueous HCl (4 mL) was sonicated for 1 min and then stirred at room temperature for 48 h. The precipitate was collected, washed with water, and dried to give **140** (25 mg, 97%) as a white solid. HPLC: rt 5.6 min (99% purity). ¹H NMR (400 MHz, DMSO-*d*₆): δ 8.79 (s, 1H), 8.28 (s, 2H), 7.98 (d, $J = 2.3$ Hz, 1H), 7.80 (dd, $J = 8.6, 2.3$ Hz, 1H), 7.56 (d, $J = 8.6$ Hz, 1H), 3.30 – 3.18 (m, 1H), 2.61 (td, $J = 14.2, 6.0$ Hz, 2H), 2.29 (d, $J = 14.5$ Hz, 2H), 2.10 (d, $J = 2.9$ Hz, 2H), 1.94 (qd, $J = 13.0, 4.0$ Hz, 2H). MS: m/z 353.1 (M+H)⁺.

Method I: Vilsmeier homologation of (2-hydroxyaryl)ethan-1-ones to 4-oxo-4H-chromene-3-carbaldehydes[35]

1.6 7-Bromo-4-oxo-4H-chromene-3-carbaldehyde (12a; Scheme 2): POCl₃ (12 mL, 129 mmol) was added slowly over 30 min to a well stirred and cooled (0–5 °C) solution of 1-(4-bromo-2-hydroxyphenyl)ethan-1-one (**11a**; 5.0 g, 23.25 mmol) in *N,N*-dimethylformamide (40 mL). After stirring at room temperature for 17 h, the suspension was poured into crushed ice and maintained at 0 °C for 1 h. The precipitated solids were collected, washed with water, and dried to give **12a** (5.2 g, 88%) as a light orange solid. ¹H

NMR (500 MHz, chloroform-*d*) δ 10.36 (d, J = 1.2 Hz, 1H), 8.51 (d, J = 1.2 Hz, 1H), 8.16 (dd, J = 8.5, 1.2 Hz, 1H), 7.74 (t, J = 1.4 Hz, 1H), 7.63 (dt, J = 8.5, 1.5 Hz, 1H). MS m/z 252.95, 254.9474 (M+1)⁺.

1.7 6-Bromo-7-fluoro-4-oxo-4H-chromene-3-carbaldehyde (12b; Scheme 2): Made from **11b** under the same conditions as described for the synthesis of **12a** to give **12b** (0.85 g, 73%) as a light orange solid. ¹H NMR (400 MHz, chloroform-*d*) δ 10.35 (s, 1H), 8.53 (d, J = 7.1 Hz, 2H), 7.33 (d, J = 7.9 Hz, 1H). MS m/z 270.9399, 272.9379 (M+1)⁺.

1.8 6-Bromo-4-oxo-4H-pyran[2,3-*c*]pyridine-3-carbaldehyde (12c; Scheme 2): To a solution of compound 1-(2-bromo-5-hydroxypyridin-4-yl)ethan-1-one (**11c**)[15] (1.0 g, 4.63 mmol) in *N,N*-dimethylformamide (12 mL) was added *tert*-butoxybis(dimethylamino)methane (3.63 g, 20.83 mmol) and the mixture was heated at 45 °C for 16 h. The mixture was concentrated and the residue was dissolved in dichloromethane and directly purified by flash silica gel column chromatography (elution with 1% methanol in dichloromethane). Fractions with yellow color (~250 mL) were collected and evaporated to give crude (*E*)-1-(2-bromo-5-hydroxypyridin-4-yl)-3-(dimethylamino)prop-2-en-1-one (0.75 g, 60%) as a light orange solid. This solid was added to Vilsmeier reagent, which was prepared by adding trifluoromethanesulfonic anhydride (1.17 g, 4.15 mmol) dropwise to ice-cold anhydrous *N,N*-dimethylformamide (7.04 mL) followed by stirring at 0 °C for 5 min. The resulting mixture was stirred at room temperature for 3 h, poured into water (25 mL) and extracted with dichloromethane (3x). The combined organic phases were dried and concentrated to give **12c** (620 mg, 88%) as a solid. ¹H NMR (400 MHz, chloroform-*d*) δ 10.33 (s, 1H), 8.85 (d, J = 0.7 Hz, 1H), 8.60 (s, 1H), 8.27 (d, J = 0.7 Hz, 1H). MS m/z 253.9446, 255.9426 (M+H)⁺.

1.9 5-Bromo-4-oxo-4H-chromene-3-carbaldehyde (86; Scheme 3): Made from **85** under the same conditions as described for the synthesis of **12a** to give **86** (2.78 g, 94%) as an off-white solid. ¹H NMR (500 MHz, chloroform-*d*): δ 10.36 (s, 1H), 8.47 (s, 1H), 7.73 (dd, J = 7.0, 2.0 Hz, 1H), 7.55 – 7.49 (m, 2H). MS: m/z 252.9491, 254.9471 (M+H)⁺.

1.10 4-Oxo-5-(prop-1-en-2-yl)-4H-chromene-3-carbaldehyde (93; Scheme 3): Made from **92** under the same conditions as described for the synthesis of **12a** to give **93** (0.427 g, 88%) as a red-brown solid. ¹H NMR (400 MHz, chloroform-*d*): δ 10.35 (s, 1H), 8.49 (s, 1H), 7.73 – 7.59 (m, 1H), 7.46 (dd, J = 8.4, 1.2 Hz, 1H), 7.21 (dd, J = 7.5, 1.2 Hz, 1H), 5.26 – 5.16 (m, 1H), 4.86 (s, 1H), 2.14 (t, J = 1.1 Hz, 3H). MS: m/z 215.0704 (M+H)⁺.

1.11 5-Isopropyl-4-oxo-4H-chromene-3-carbaldehyde (95; Scheme 3): Made from **94** under the same conditions as described for the synthesis of **12a** to give **95** (0.29 g, 67%) as an orange solid. ¹H NMR (500 MHz, chloroform-*d*): δ 10.36 (d, J = 4.4 Hz, 1H), 8.43 (d, J = 4.3 Hz, 1H), 7.64 (td, J = 8.1, 4.2 Hz, 1H), 7.46 (dd, J = 7.7, 3.5 Hz, 1H), 7.36 – 7.32 (m, 1H), 4.71 – 4.62 (m, 1H), 1.31 (dd, J = 6.8, 4.3 Hz, 6H). MS: m/z 217.0859 (M+H)⁺.

1.12 6-(Dimethylamino)-4-oxo-4H-chromene-3-carbaldehyde (98a; Scheme 4): Made from POCl₃ (10.7 g, 69.7 mmol), compound **97a** (2.5 g, 13.95 mmol) and *N,N*-dimethylformamide (14 mL) as described for the synthesis of **12a** except that after

quenching the reaction by addition to ice water, the pH was adjusted to ~8.5 with saturated aq. Na₂CO₃. Extraction with dichloromethane (3x) followed by further standard workup gave a dark brown solid that was purified by flash silica gel chromatography, eluting with 20:10:3 hexanes/ethyl acetate/dichloromethane, to give **98a** (2.06 g, 68%) as a solid. ¹H NMR (400 MHz, chloroform-*d*) δ 10.41 (s, 1H), 8.50 (s, 1H), 7.42 (d, *J* = 9.2 Hz, 1H), 7.36 (d, *J* = 3.2 Hz, 1H), 7.13 (dd, *J* = 9.2, 3.2 Hz, 1H), 3.07 (s, 6H). MS *m/z* 218.0 (M+H)⁺.

1.13 6-Morpholino-4-oxo-4H-chromene-3-carbaldehyde (98b; Scheme 4): Made from compound **97b** as described for the synthesis of **98a** to give **98b** (1.66 g, 68%) as a red-brown solid. ¹H NMR (400 MHz, chloroform-*d*): δ 10.40 (s, 1H), 8.52 (s, 1H), 7.61 (d, *J* = 3.1 Hz, 1H), 7.47 (d, *J* = 9.2 Hz, 1H), 7.34 (dd, *J* = 9.2, 3.1 Hz, 1H), 3.92 – 3.88 (m, 4H), 3.29 – 3.23 (m, 4H). MS: *m/z* 260.0 (M+H)⁺.

Method J: Oximation of 4-oxo-4H-chromene-3-carbaldehydes[14, 36]

1.14 7-Bromo-4-oxo-4H-chromene-3-carbaldehyde oxime (13a; Scheme 2): A suspension of compound **12a** (200 mg, 0.79 mmol), hydroxylamine hydrochloride (65.9 mg, 0.95 mmol) and ethanol (4 mL) was stirred at 60 °C for 1 h. The mixture was then maintained at 0 °C for 30 min and the solids were collected, washed with ethanol, and dried to leave **13a** (170 mg, 80%) as an off-white solid. ¹H NMR (400 MHz, DMSO-*d*₆) δ 11.46 (s, 1H), 8.66 (d, *J* = 0.8 Hz, 1H), 8.05 (d, *J* = 1.9 Hz, 1H), 8.05 (d, *J* = 0.8 Hz, 1H), 8.00 (d, *J* = 8.5 Hz, 1H), 7.70 (dd, *J* = 8.5, 1.8 Hz, 1H). MS *m/z* 267.9603, 269.9583 (M+H)⁺.

1.15 6-Bromo-7-fluoro-4-oxo-4H-chromene-3-carbaldehyde oxime (13b; Scheme 2): Made from **12b** under the same conditions as described for the synthesis of **13a** to give **13b** (593 mg, 66%) as an off-white solid. ¹H NMR (400 MHz, DMSO-*d*₆) δ 11.50 (s, 1H), 8.72 (d, *J* = 0.8 Hz, 1H), 8.32 (d, *J* = 7.7 Hz, 1H), 8.04 (d, *J* = 0.8 Hz, 1H), 7.95 (d, *J* = 9.1 Hz, 1H). MS *m/z* 285.9511, 287.9490 (M+H)⁺.

1.16 6-Bromo-4-oxo-4H-pyrano[2,3-*c*]pyridine-3-carbaldehyde oxime (13c; Scheme 2): Made from **12c** under the same conditions as described for the synthesis of **13a** to give **13c** (130 mg, 61%) as an off-white solid. ¹H NMR (400 MHz, DMSO-*d*₆) δ 11.59 (s, 1H), 9.05 (s, 1H), 8.81 (s, 1H), 8.09 (s, 1H), 8.04 (s, 1H). MS *m/z* 268.9556, 270.9537 (M+H)⁺.

1.17 5-Bromo-4-oxo-4H-chromene-3-carbaldehyde oxime (87; Scheme 3): Made from **86** under the same conditions as described for the synthesis of **13a** to give **87** (2.28 g, 77%) as a white solid. ¹H NMR (400 MHz, DMSO-*d*₆): δ 12.20 (s, 1H), 9.50 (s, 1H), 7.75 (dd, *J* = 6.7, 2.3 Hz, 1H), 7.70 – 7.64 (m, 2H), 7.57 (s, 1H). MS: *m/z* 267.9601, 269.9583 (M+H)⁺.

Method K: Conversion of 4-oxo-4H-chromene-3-carbaldehyde oximes to 4-oxo-4H-chromene-3-carbonitriles[36]

1.18 7-Bromo-4-oxo-4H-chromene-3-carbonitrile (14a; Scheme 2): A suspension of compound **13a** (165 mg, 0.62 mmol) in acetic anhydride (3 mL) was stirred at 110 °C for 18 h. The mixture was concentrated to leave **14a** (150 mg, 97%) as an off-white solid. ¹H NMR (400 MHz, chloroform-*d*) δ 8.39 (s, 1H), 8.12 (d, *J* = 8.5 Hz, 1H), 7.75 (d, *J* = 1.8 Hz, 1H), 7.66 (dd, *J* = 8.5, 1.7 Hz, 1H). MS *m/z* 249.9497, 251.9477 (M+H)⁺.

1.19 6-Bromo-7-fluoro-4-oxo-4H-chromene-3-carbonitrile (14b; Scheme 2): Made from **13b** under the same conditions as described for the synthesis of **14a** to give **14b** (0.52 g, 94%) as an off-white solid. ¹H NMR (500 MHz, chloroform-*d*) δ 8.50 (d, *J* = 7.4 Hz, 1H), 8.40 (s, 1H), 7.34 (d, *J* = 7.8 Hz, 1H). MS *m/z* 267.9404, 269.9384 (M+H)⁺.

1.20 6-Bromo-4-oxo-4H-pyran[2,3-*c*]pyridine-3-carbonitrile (14c; Scheme 2): Made from **13c** under the same conditions as described for the synthesis of **14a** to give **14c** (115 mg, 99%) as an orange solid. ¹H NMR (400 MHz, chloroform-*d*) δ 8.87 (d, *J* = 0.7 Hz, 1H), 8.50 (s, 1H), 8.23 (d, *J* = 0.7 Hz, 1H). MS *m/z* 250.9449, 252.9430 (M+H)⁺.

1.21 5-Bromo-4-oxo-4H-chromene-3-carbonitrile (88; Scheme 3): Made from **87** under the same conditions as described for the synthesis of **14a** to give **88** (2.1 g, 99%) as an off-white solid. ¹H NMR (400 MHz, chloroform-*d*): δ 8.34 (s, 1H), 7.77 (dd, *J* = 7.6, 1.4 Hz, 1H), 7.59 – 7.49 (m, 2H). MS: *m/z* 249.9497, 251.9475 (M+H)⁺.

1.22 6-(Dimethylamino)-4-oxo-4H-chromene-3-carbonitrile (99a; Scheme 4): A mixture of **98a** (2.02 g, 9.30 mmol), hydroxylamine hydrochloride (0.775 g, 11.2 mmol) and sodium iodide (0.697 g, 4.65 mmol) in acetonitrile (35 mL) was heated at reflux for 2 h. The cooled mixture was filtered and the collected solids were washed with acetonitrile and dichloromethane. The combined filtrates were concentrated to a residual solid that was diluted with water and extracted with dichloromethane (3x). The combined extracts were washed successively with 5% aq. sodium sulfate, water, and brine, then dried and concentrated to leave **99a** (0.68 g, 34%) as an orange solid that was used directly in the next step. MS *m/z* 215.0 (M+H)⁺.

1.23 6-Morpholino-4-oxo-4H-chromene-3-carbonitrile (99b; Scheme 4): Reaction of compound **98b** as described for the synthesis of **99a** (heating for 3 h) gave **99b** (1.68 g, 58%) as a brown solid that was used directly in the next step. MS *m/z* 257.0 (M+H)⁺.

Method L: Annulation of 4-oxo-4H-chromene-3-carbonitriles to ethyl 2-amino-5-oxo-5H-chromeno[2,3-*b*]pyridine-3-carboxylates[14]

1.24 Ethyl 2-amino-8-bromo-5-oxo-5H-chromeno[2,3-*b*]pyridine-3-carboxylate (6; Scheme 2): A mixture of compound **14a** (140 mg, 0.56 mmol), ethyl cyanoacetate (82 mg, 0.73 mmol), piperidine (48.6 mg, 0.57 mmol) and ethanol (4 mL) was heated at reflux for 2 h. After standing overnight at room temperature, the precipitated solids were collected, washed with ethanol, and dried to afford **6** (190 mg, 93%) as a white solid. ¹H NMR (500 MHz, chloroform-*d*) δ 9.13 (s, 1H), 8.41 (s, 1H), 8.13 (d, *J* = 8.4 Hz, 1H), 7.68 (d, *J* = 1.7 Hz, 1H), 7.53 (dd, *J* = 8.4, 1.8 Hz, 1H), 5.90 (s, 1H), 4.41 (q, *J* = 7.1 Hz, 2H), 1.44 (t, *J* = 7.1 Hz, 3H). MS *m/z* 362.9973, 364.9954 (M+H)⁺.

1.25 Ethyl 2-amino-7-bromo-8-fluoro-5-oxo-5H-chromeno[2,3-*b*]pyridine-3-carboxylate (7; Scheme 2): Made from **14b** under the same conditions as described for the synthesis of **6** (heating for 3 h) to give **7** (666 mg, 90%) as an off-white solid. ¹H NMR (400 MHz, chloroform-*d*) δ 9.13 (s, 1H), 8.49 (d, *J* = 7.6 Hz, 1H), 8.44 (s, 1H), 7.27 (d, *J* = 7.6

Hz, 1H), 5.90 (s, 1H), 4.41 (q, $J = 7.1$ Hz, 2H), 1.44 (t, $J = 7.1$ Hz, 3H). MS m/z 380.9980, 382.9861 (M+H)⁺.

1.26 Ethyl 2-amino-7-bromo-5-oxo-5H-pyrano[2,3-b:6,5-c']dipyridine-3-carboxylate (8; Scheme 2): Made from **14c** under the same conditions as described for the synthesis of **6** to give **8** (130 mg, 77%) as a light orange solid. ¹H NMR (400 MHz, chloroform-*d*) δ 9.11 (s, 1H), 8.77 (s, 1H), 8.54 (s, 1H), 8.22 (s, 1H), 6.02 (s, 1H), 4.42 (q, $J = 7.2$ Hz, 2H), 1.44 (t, $J = 7.1$ Hz, 3H). MS m/z 363.9928, 365.9912 (M+H)⁺.

1.27 Ethyl 2-amino-7-bromo-5-oxo-5H-chromeno[2,3-b]pyridine-3-carboxylate (9): Compound **9** was prepared as described by Ghosh *et al.*[16]

1.28 Ethyl 2-amino-5-oxo-6-(prop-1-en-2-yl)-5H-chromeno[2,3-b]pyridine-3-carboxylate (90; Scheme 3): Made from **89** under the same conditions as described for the synthesis of **6** (heating for 3 h) to give **90** (510 mg, 73%). ¹H NMR (400 MHz, chloroform-*d*): δ 9.13 (s, 1H), 8.33 (s, 1H), 7.62 (dd, $J = 8.4, 7.4$ Hz, 1H), 7.45 (dd, $J = 8.4, 1.2$ Hz, 1H), 7.12 (dd, $J = 7.4, 1.2$ Hz, 1H), 5.84 (s, 1H), 5.17 (t, $J = 1.7$ Hz, 1H), 4.89 – 4.81 (m, 1H), 4.37 (q, $J = 7.2$ Hz, 2H), 2.16 (t, $J = 1.1$ Hz, 3H), 1.40 (t, $J = 7.1$ Hz, 3H). MS: m/z 325.1184 (M+H)⁺.

1.29 Ethyl 2-amino-7-(dimethylamino)-5-oxo-5H-chromeno[2,3-b]pyridine-3-carboxylate (100a; Scheme 4): Made from **99a** under the same conditions described for the synthesis of **6** (heating for 2.5 h) to give **100a** (302 mg, 58%) as yellow solid. ¹H NMR (400 MHz, DMSO-*d*₆) δ 8.80 (s, 1H), 8.27 (s, 1H), 8.04 (s, 1H), 7.46 (d, $J = 9.2$ Hz, 1H), 7.30 (dd, $J = 9.2, 3.2$ Hz, 1H), 7.17 (d, $J = 3.2$ Hz, 1H), 4.35 (q, $J = 7.1$ Hz, 2H), 2.97 (s, 6H), 1.36 (t, $J = 7.1$ Hz, 3H). MS m/e 328.0 (M+H)⁺.

1.30 Ethyl 2-amino-7-morpholino-5-oxo-5H-chromeno[2,3-b]pyridine-3-carboxylate (100b; Scheme 4): Made from **99b** under the same conditions described for the synthesis of **100a** (heating for 4 h) to give **100b** (0.235 g, 9% over two steps). ¹H NMR (400 MHz, chloroform-*d*): δ 9.15 (s, 1H), 7.65 (d, $J = 3.1$ Hz, 1H), 7.44 (d, $J = 9.1$ Hz, 1H), 7.34 (dd, $J = 9.2, 3.1$ Hz, 1H), 4.41 (q, $J = 7.1$ Hz, 2H), 3.94 – 3.84 (m, 4H), 3.27 – 3.20 (m, 4H), 1.44 (t, $J = 7.1$ Hz, 3H). MS: m/z 370.0 (M+H)⁺.

1.31 2-Amino-7-(dimethylamino)-5-oxo-5H-chromeno[2,3-b]pyridine-3-carbonitrile (104a; Scheme 4): A solution of **99a** (150 mg, 0.70 mmol), piperidine (79 mg, 0.93 mmol), malononitrile (123 mg, 1.86 mmol) and ethanol (3 mL) was heated at reflux for 3 h. The cooled mixture was stored overnight at room temperature and the precipitate was collected, washed with ethanol, and dried to afford **104a** (140 mg, 71%). ¹H NMR (400 MHz, DMSO-*d*₆) δ 8.60 (s, 1H), 7.46 (d, $J = 9.2$ Hz, 1H), 7.29 (dd, $J = 9.2, 3.2$ Hz, 1H), 7.14 (d, $J = 3.2$ Hz, 1H), 2.97 (s, 6H). MS m/e 281.1 (M+H)⁺.

1.32 2-Amino-7-morpholino-5-oxo-5H-chromeno[2,3-b]pyridine-3-carbonitrile (104b; Scheme 4): Made from **99b** under the same conditions described for the synthesis of **104a** to give **104b** (0.37 g, 65%). ¹H NMR (400 MHz, DMSO-*d*₆): δ 8.62 (s, 1H), 7.54 (d, $J = 2.8$

Hz, 1H), 7.52 (s, 1H), 7.50 (s, 1H), 7.39 (d, $J = 2.9$ Hz, 1H), 3.76 (d, $J = 5.0$ Hz, 4H), 3.18 (d, $J = 4.8$ Hz, 4H). MS: m/z 323.1 (M+H)⁺.

Method M: Tetrazoles from nitriles:

1.33 2-Amino-7-(cyclohex-1-en-1-yl)-3-(1H-tetrazol-5-yl)-5H-chromeno[2,3-*b*]pyridine-5-one (169; Scheme 4): A mixture of compound **102** (50 mg, 0.16 mmol), sodium azide (30.7 mg, 0.47 mmol), and ammonium chloride (25.3 mg, 0.47 mmol) in *N,N*-dimethylformamide (0.5 mL) was stirred at 90 °C in a capped vial for 18 h. After cooling, the mixture was poured into water and the suspension was acidified with 10% aq HCl to pH 2–3 followed by stirring at room temperature overnight. The precipitate was collected, washed successively with water, acetonitrile, and dichloromethane, and dried to give **169** (45 mg, 79%). HPLC: rt 7.4 min (90% purity). ¹H NMR (400 MHz, DMSO-*d*₆): δ 8.99 (s, 1H), 8.44 (s, 2H), 8.01 (d, $J = 2.4$ Hz, 1H), 7.89 (dd, $J = 8.8, 2.4$ Hz, 1H), 7.55 (d, $J = 8.8$ Hz, 1H), 6.29 (s, 1H), 2.42 (s, 2H), 2.21 (d, $J = 4.6$ Hz, 2H), 1.76 (dd, $J = 7.2, 4.6$ Hz, 2H), 1.68 – 1.55 (m, 2H). MS: m/z 361.0 (M+H)⁺.

1.34 2-Amino-7-cyclohexyl-3-(1H-tetrazol-5-yl)-5H-chromeno[2,3-*b*]pyridine-5-one (168; Scheme 4): Made from **103** under the same conditions described for the synthesis of **169** to give **168** (38 mg, 84%) as an orange solid. HPLC: rt 7.6 min (95% purity). ¹H NMR (400 MHz, DMSO-*d*₆): δ 9.02 (s, 1H), 8.44 (s, 2H), 7.93 (d, $J = 2.2$ Hz, 1H), 7.76 – 7.67 (m, 1H), 7.55 (d, $J = 8.5$ Hz, 1H), 2.67 (t, $J = 11.0$ Hz, 1H), 1.82 (d, $J = 11.0$ Hz, 4H), 1.72 (d, $J = 12.5$ Hz, 1H), 1.43 (q, $J = 13.6, 13.0$ Hz, 4H), 1.27 (d, $J = 12.0$ Hz, 1H). MS: m/z 363.1 (M+H)⁺.

1.35 2-Amino-7-(dimethylamino)-3-(1H-tetrazol-5-yl)-5H-chromeno[2,3-*b*]pyridin-5-one (170; Scheme 4): Made from **104a** under the same conditions described for the synthesis of **169** (heating for 16 h) to leave a crude solid that was suspended in methanol (5 mL) and sonicated at room temperature for 5 min. The solids were collected, washed with methanol and ether, and dried to give **170** (40 mg, 27%) as a red-brown solid. HPLC: rt 4.4 min (87% purity). ¹H NMR (400 MHz, DMSO-*d*₆) δ 9.00 (s, 1H), 8.46 – 8.30 (m, 2H), 7.49 (d, $J = 9.1$ Hz, 1H), 7.30 (d, $J = 9.4$ Hz, 1H), 7.20 (s, 1H), 2.98 (s, 6H). MS: m/z 324.0 (M+H)⁺.

1.36 2-Amino-7-morpholino-3-(1H-tetrazol-5-yl)-5H-chromeno[2,3-*b*]pyridine-5-one (171; Scheme 4): Made from **104b** under the same conditions described for the synthesis of **170** to give **171** (58 mg, 58%). ¹H NMR (400 MHz, DMSO-*d*₆): δ 9.02 (s, 1H), 8.41 (s, 1H), 7.55 (s, 1H), 7.45 (s, 1H), 3.78 (m, 4H), 3.19 (m, 4H). MS: m/z 366.1 (M+H)⁺.

Method N: 5-aminotetrazole amide from carboxylic acid:

1.37 2-Amino-7-morpholino-5-oxo-*N*-(1H-tetrazol-5-yl)-5H-chromeno[2,3-*b*]pyridine-3-carboxamide (172; Scheme 4): To a stirred suspension of compound **151** (100 mg, 0.29 mmol) and *N,N*-dimethylformamide (2 mg, catalytic) in dry dichloromethane (10 mL) at room temperature was added drop-wise thionyl chloride (4 mL, 55.7 mmol), and the resulting mixture was heated at reflux for 3 h. The cooled mixture was concentrated and dried *in vacuo* to give crude 2-amino-7-morpholino-5-oxo-5H-chromeno[2,3-*b*]pyridine-3-

carbonyl chloride (154 mg) as an orange solid. A solution of this (105 mg, 0.29 mmol), tetrazole-5-amine (37 mg, 0.44 mmol), triethylamine (178 mg, 1.76 mmol) and pyridine (5 mL) was stirred at room temperature for 4 h. The mixture was diluted with acetonitrile (10 mL), stirred for 5 min and filtered. The filtrate was concentrated to a residue that was diluted with water (5 mL) and dichloromethane (5 mL). The biphasic mixture was sonicated for 5 min, stored at room temperature for 16 h and filtered. The collected solids were washed successively with water and dichloromethane, and dried to give **172** (45 mg, 38%). ¹H NMR (400 MHz, DMSO-*d*₆): δ 9.10 (s, 1H), 8.24 (s, 2H), 7.56 (d, *J* = 2.9 Hz, 1H), 7.54 (s, 1H), 7.45 (d, *J* = 2.8 Hz, 1H), 3.79 – 3.76 (m, 4H), 3.19 (m, 4H). MS: *m/z* 409.0 (M+H)⁺.

Biological Materials and Methods

1.38 Protein Expression and Purification.—Human TBK1 spanning residues 1–657 and IKKε spanning residues 1–655 were cloned into a modified pFastBac vector (pH7pFB, University of Michigan Center for Structural Biology) via ligation-independent cloning. Recombinant baculovirus was prepared by transfecting SF9 insect cells with purified bacmid and passaging several times to obtain virus of a higher titer. For expression, SF9 or Hi5 insect cells at a density of 2×10⁶ cells/mL were infected with baculovirus and harvested after 65–72 h. Cells were pelleted and flash frozen in liquid nitrogen.

Cell pellets were thawed and resuspended in lysis buffer (20 mM HEPES pH 8.0 for TBK1 or pH 7.5 for IKKε, 100 mM NaCl, 40 mM imidazole, 1 mM DTT, 0.1 mM phenylmethanesulfonylfluoride (PMSF), leupeptin, and lima bean trypsin protease inhibitor). Resuspended cells were homogenized with a Dounce homogenizer prior to brief sonication. The lysate was clarified by ultracentrifugation for 1 h at >200,000xg. The resulting supernatant was glass filtered prior to being slowly flowed through Ni-NTA resin. The resin was washed with lysis buffer and the protein eluted with lysis buffer supplemented with an additional 200 mM imidazole. Due to instability, IKKε was diluted 2–3 fold with a buffer lacking imidazole (20 mM HEPES pH 7.5, 200 mM NaCl, and 1 mM DTT) and concentrated to ~1 mg mL⁻¹ as determined by absorbance at 280 nm using the calculated IKKε molecular weight and molar extinction coefficient 76,610 kDa and 57,300 M⁻¹ cm⁻¹, respectively, and flash frozen in liquid nitrogen for kinase assays.

TBK1 was further purified by anion exchange chromatography using a HiTrap Q column and eluted with a NaCl gradient from 0–1.0 M at pH 8.0. TBK1 to be used for kinase assays was concentrated to ~1 mg mL⁻¹ by absorbance at 280 nm and flash frozen in liquid nitrogen. TBK1 from anion exchange to be used for crystallography was incubated at 4 °C overnight with ~10% (w/w) TEV protease while being dialyzed against 1 L of 20 mM HEPES pH 7.5, 100 mM NaCl, and 2 mM DTT in 6–8,000 kDa cutoff dialysis tubing to cleave the 6-His tag. The following day, the mixture was passed through Ni-NTA resin to remove the TEV protease. The cleaved TBK1 protein was dephosphorylated by incubating at room temperature for 4–6 h with λ phosphatase (New England Biolabs) in buffer supplemented with 1 mM MnCl₂. The dephosphorylated protein was further purified via size-exclusion chromatography on an S200 column in buffer lacking MnCl₂ (20 mM HEPES pH 7.5, 100 mM NaCl, and 1 mM DTT). Purified TBK1 for crystallography was concentrated to ~3 mg/mL as determined by absorbance at 280 nm using the calculated

TBK1 molecular weight and molar extinction coefficient 75,650 kDa and 78,730 M⁻¹ cm⁻¹, respectively, and then flash frozen in liquid nitrogen.

1.39 —Crystallization conditions were based off those previously reported with modifications.[37, 38] TBK1 crystals were grown at 20 °C via hanging drop vapor diffusion in drops containing 1 μL of 100 mM HEPES pH 7.5, 4% (w/v) PEG 8,000, 2 μL of purified human TBK1 (residues 1–657 at ~3 mg mL⁻¹), and 0.2 μL inhibitor (10 mM in DMSO) over wells containing 1 mL of 100 mM HEPES pH 7.5, 4% (w/v) PEG 8,000, and 10% DMSO. Small diamonds appeared within 1–2 d and grew for an additional 1–2 d. Better diffracting and larger crystals were obtained through microseeding. Crystals were harvested and briefly soaked in a cryoprotecting solution containing 100 mM HEPES pH 8.5, 8% (w/v) PEG 8,000, 30% (v/v) PEG 400, and 0.5 mM inhibitor prior to flash freezing in liquid nitrogen.

Data were collected at LS-CAT (Sector 21, Advanced Photon Source, Argonne National Lab) under a cryostream maintained at 100 K using an Eiger 9M or MAR300 detector. Data were processed with XDS and the structure solved in Phenix via molecular replacement using a ligand-free structure of TBK1 as the search model (PDB entry 4IM0).[39]–[40] The model was built in alternating rounds of manual model building in Coot with reciprocal space refinement in Phenix alongside validation with MolProbity.[41]–[42] Ligand restraints were generated with eLBOW. Graphics were prepared with PyMol.[43] Coordinates and diffraction amplitudes have been deposited in the PDB with the accession codes 6CQ0, 6CQ4, and 6CQ5 for the **114**, **131**, and **150** structures, respectively.

1.40 Thermodynamic solubility studies.—Thermodynamic solubility was evaluated by Analiza (Cleveland, OH) using their standard protocol with a CLND detector. Compounds were dissolved in 450 μL PBS pH 7.4 and shaken overnight at room temperature. The solution was filtered through a 0.45 μm filter and injected directly into the CLND. Concentrations were determined via calibration curves. Results are shown in Table SM2.

1.41 IC₅₀ Determination by Radiometric Kinase Assay.—Reactions containing 50 nM TBK1 or IKKe and 5 μM myelin basic protein (MyBP) in reaction buffer (50 mM HEPES pH 7.5, 10 mM NaCl, 10 mM MgCl₂, and 1 mM DTT) with varying concentrations of inhibitor were initiated with 5 μM ATP spiked with [γ -³²P]-ATP (Perkin Elmer) and allowed to proceed for 30 min at room temperature in a final volume of 20 μL. Reactions were quenched with SDS gel loading dye, run on 4–15% SDS-PAGE gels, and imaged on phosphor screens. Band intensities corresponding to phosphorylated MyBP were quantified with ImageQuant and the data analyzed in GraphPad Prism 7 using a three parameter dose-response curve model with the Hill slope constrained to -1.

1.42 3T3-L1 differentiation.—3T3-L1 fibroblasts (American Type Culture Collection) were cultured in DMEM containing 10% FBS. Once grown to confluence, adipocyte differentiation was initiated using a three component cocktail containing 500 μM 3-isobutyl-1-methylxanthine, 250 nM dexamethasone and 1 μg ml⁻¹ insulin for 3 d, followed by an additional 3 d of media containing insulin and finally differentiation was completed in the culture media. Only cultures in which >90% of cells displayed adipocyte morphology

were used. Fully differentiated adipocytes, which had been cultured in the FBS only media for 1 wk, were treated with 100 μ M amlexanox analogue, amlexanox or vehicle control. Cells were harvested after 1 h of treatment for western blot analysis. Media was collected after 4 h of treatment for IL-6 measurement.

1.43 Western blot analysis.—Tissues were homogenized in lysis buffer (50 mM Tris pH 7.5, 150 mM NaCl, 2 mM EDTA, 10% glycerol, 1% Triton X-100, 1 mM DTT, 1 mM Na_3VO_4 , 5 mM NaF, 1 mM phenylmethanesulfonylfluoride, 25 mM glycerol 2-phosphate and freshly added protease inhibitor tablet) and then incubated them for 1 h at 4 °C. Cell lysates were produced in an SDS lysis buffer (100 mM Tris pH 7.5, 130 mM NaCl, 1% NP-40, 0.1% SDS, 0.2% sodium deoxycholate, 1 mM Na_3VO_4 , 1 mM NaF, 100 mM $\text{Na}_4\text{P}_2\text{O}_7$, 1 mM phenylmethanesulfonylfluoride, 25 mM glycerol 2-phosphate and freshly added protease inhibitor tablet) and sonicated for three 5 s pulses at an output power of 6. Crude lysates were centrifuged at 14,000 *g* for 15 min twice and the protein concentration was determined using Bio-Rad Protein Assay Dye Reagent. Samples were diluted in SDS sample buffer. Bound proteins were resolved by SDS–PAGE and transferred to nitrocellulose membranes (Bio-Rad). Individual proteins were detected with specific antibodies and visualized on film using horseradish peroxidase-conjugated secondary antibodies (Bio-Rad) and Western Lightning Enhanced Chemiluminescence (Perkin Elmer Life Sciences). TBK1 (3013), phosphorylated TBK1 (Ser172–5483), p38 (9212), and phosphorylated p38 (Thr180/Tyr182–9211)-specific antibodies were purchased from Cell Signaling Technology (Danvers, MA).

1.44 IL-6 measurement.—Mouse IL-6 levels were quantified using Mouse IL-6 Quantikine ELISA from R&D (SM6000B), with 50 μ L of serum or cell culture media.

1.45 Animal studies.—Wild-type male C57Bl/6 mice were fed a high fat diet consisting of 45% of calories from fat (D12451 Research Diets Inc.) starting at 8 weeks of age for 3 months to induce metabolic disease. After 1-wk gavage conditioning the mice were treated by oral gavage with vehicle, amlexanox and amlexanox analogues at a dose of 25 mg kg^{-1} . Serum IL-6 levels were measured 4 h after the first dose, when the response to amlexanox is at its highest. The insulin tolerance test was performed on the day of the third treatment: Fasting blood glucose levels from tail blood were measured after a 3 h fast, using the OneTouch Ultra glucometer (Lifescan). Mice were then given an intraperitoneal injection of insulin at a dose of 0.75 Units kg^{-1} body weight. Blood glucose levels were measured again at 20, 40, and 60 min post injection. Negative controls (vehicle) and positive controls (amlexanox) were included in all experiments. Analogue treated mice were closely and frequently observed and then necropsied to identify any potential harmful side effects. Mice were assigned to treatment groups, such that prior to treatment the mean body weight, as well as the standing deviation of the body weight, was equal across treatment groups, using a method similar to block randomization. All animal use was in compliance with the Institute of Laboratory Animal Research Guide for the Care and Use of Laboratory Animals and approved by the University Committee on Use and Care of Animals at the University of Michigan and was in accordance with UC San Diego and Institutional Animal Care and Use

Committee-approved protocols. The studies also conformed to the NIH Guide for Care and Use of Laboratory Animals of the NIH.

Supplementary Material

Refer to Web version on PubMed Central for supplementary material.

Acknowledgements

This study was supported by National Institutes of Health (NIH) Pharmacological Sciences Training Program fellowship (T32-GM007767), U.S. Department of Education GAANN fellowship (P200A150164), and NIH R01 (HL122416, HL071818, DK100319) and K01 (DK105075, DK060591) grants. This research used resources of the Advanced Photon Source (DOE) under Contract No. DE-AC02-06CH11357. Use of the LS-CAT Sector 21 was supported by the Michigan Economic Development Corporation and the Michigan Technology Tri-Corridor (Grant 085P1000817).

References

- [1]. Giordano A, Frontini A, Cinti S, Convertible visceral fat as a therapeutic target to curb obesity, *Nat. Rev. Drug Discovery*, 15 (2016) 405–424. [PubMed: 26965204]
- [2]. Omran Z, Obesity: Current Treatment and Future Horizons, *Mini-Rev. Med. Chem*, 17 (2017) 51–61. [PubMed: 27320641]
- [3]. Saltiel AR, New therapeutic approaches for the treatment of obesity, *Science Translational Medicine*, 8 (2016) 1–11.
- [4]. Dietrich MO, Horvath TL, Limitations in anti-obesity drug development: the critical role of hunger-promoting neurons, *Nat. Rev. Drug Discovery*, 11 (2012) 675–691. [PubMed: 22858652]
- [5]. Thomsen WJ, Grottick AJ, Menzaghi F, Reyes-Saldana H, Espitia S, Yuskin D, Whelan K, Martin M, Morgan M, Chen W, Al-Shamma H, Smith B, Chalmers D, Behan D, Lorcaserin, a novel selective human 5-hydroxytryptamine_{2C} agonist: in vitro and in vivo pharmacological characterization, *J. Pharmacol. Exp. Ther.*, 325 (2008) 577–587. [PubMed: 18252809]
- [6]. Chandra S, Jyothi M, Raghu MRP, Clinical treatment of obesity disease: a brief review of orlistat, *World J. Pharm. Pharm. Sci*, 4 (2015) 448–465.
- [7]. Clapham JC, Arch JRS, Targeting thermogenesis and related pathways in anti-obesity drug discovery, *Pharmacol. Ther.*, 131 (2011) 295–308. [PubMed: 21514319]
- [8]. Chiang S-H, Bazuine M, Lumeng CN, Geletka LM, Mowers J, White NM, Ma J-T, Zhou J, Qi N, Westcott D, Delproposito JB, Blackwell TS, Yull FE, Saltiel AR, The protein kinase IKK ϵ regulates energy balance in obese mice, *Cell (Cambridge, MA, U. S.)*, 138 (2009) 961–975.
- [9]. Saltiel AR, Insulin Resistance in the Defense against Obesity, *Cell Metab*, 15 (2012) 798–804. [PubMed: 22682220]
- [10]. Oral EA, Reilly SM, Gomez AV, Meral R, Butz L, Ajluni N, Chenevert TL, Korytnaya E, Neidert AH, Hench R, Rus D, Horowitz JF, Poirier B, Zhao P, Lehmann K, Jain M, Yu R, Liddle C, Ahmadian M, Downes M, Evans RM, Saltiel AR, Inhibition of IKK ϵ and TBK1 Improves Glucose Control in a Subset of Patients with Type 2 Diabetes, *Cell Metab*, 26 (2017) 157–170.e157. [PubMed: 28683283]
- [11]. Beyett TS, Gan X, Reilly SM, Chang L, Gomez AV, Saltiel AR, Showalter HD, Tesmer JGG, Carboxylic acid derivatives of amlexanox display enhanced potency towards TBK1 and IKK ϵ and reveal mechanisms for selective inhibition, *Mol. Pharm*, 94 (2018) 1210–1219.
- [12]. Nohara A, Umetani T, Sanno Y, Antianaphylactic agents. I. Facile synthesis of 4-oxo-4H-1-benzopyran-3-carboxaldehydes by Vilsmeier reagents, *Tetrahedron*, 30 (1974) 3553–3561.
- [13]. Reddy GJ, Latha D, Thirupathaiiah C, Rao KS, An efficient one step conversion of 3-formylchromones into 3-cyanochromones, *Org. Prep. Proced. Int*, 36 (2004) 287–289.
- [14]. Nohara A, Ishiguro T, Ukawa K, Sugihara H, Maki Y, Sanno Y, Studies on antianaphylactic agents. 7. Synthesis of antiallergic 5-oxo-5H-[1]benzopyrano[2,3-b]pyridines, *J. Med. Chem*, 28 (1985) 559–568. [PubMed: 3989816]

- [15]. Hunt KW, Rizzi JP, Cook A, Preparation of spirochromanimidazolone derivatives for use as beta-secretase inhibitors, PCT Int. Appl. WO2011072064 A1 (2011).
- [16]. Ghosh C, Sinharoy DK, Mukhopadhyay KK, Heterocyclic systems. Part 6. Reactions of 4-oxo-4H-[1]benzopyran-3-carbonitriles with hydrazine, phenylhydrazine, hydroxylamine, and some reactive methylene compounds, J. Chem. Soc., Perkin Trans 1, (1979) 1964–1968.
- [17]. Penner M, Rauniyar V, Kaspar LT, Hall DG, Catalytic Asymmetric Synthesis of Palmerolide A via Organoboron Methodology, J. Am. Chem. Soc, 131 (2009) 14216–14217. [PubMed: 19764721]
- [18]. Xiao Y, Kellar KJ, Brown ML, Paige MA, Liu Y, Levin ED, Rezvani AH, 2,5-Disubstitutedpyridyl nicotinic ligands and methods of use, US Patent 9303017 B2 (2016).
- [19]. Oslob JD, McDowell RS, Johnson R, Yang H, Evanchik M, Zaharia CA, Cai H, Hu LW, Preparation of heterocyclic-fused imidazole benzoylpiperidine derivatives as modulators of lipid synthesis, PCT Int. Appl. WO2012122391 A1 (2012)
- [20]. Denmark SE, Venkatraman S, On the Mechanism of the Skraup-Doebner-Von Miller Quinoline Synthesis, J. Org. Chem, 71 (2006) 1668–1676. [PubMed: 16468822]
- [21]. Harris MC, Huang X, Buchwald SL, Improved Functional Group Compatibility in the Palladium-Catalyzed Synthesis of Aryl Amines, Org. Lett, 4 (2002) 2885–2888. [PubMed: 12182580]
- [22]. Beria I, Bossi RT, Brasca MG, Caruso M, Ceccarelli W, Fachin G, Fasolini M, Forte B, Fiorentini F, Pesenti E, Pezzetta D, Posterì H, Scolaro A, Depaolini SR, Valsasina B, NMS-P937, a 4,5-dihydro-1H-pyrazolo[4,3-h]quinazoline derivative as potent and selective Polo-like kinase 1 inhibitor, Bioorg. Med. Chem. Lett, 21 (2011) 2969–2974. [PubMed: 21470862]
- [23]. Mowers J, Uhm M, Reilly SM, Simon J, Leto D, Chiang SH, Chang L, Saltiel AR, Inflammation produces catecholamine resistance in obesity via activation of PDE3B by the protein kinases IKK{varepsilon} and TBK1, Elife, 2 (2013) e01119. [PubMed: 24368730]
- [24]. Zhao P, Wong K.i., Sun X, Reilly SM, Uhm M, Liao Z, Skorobogatko Y, Saltiel AR, TBK1 at the Crossroads of Inflammation and Energy Homeostasis in Adipose Tissue, Cell (Cambridge, MA, U. S.), 172 (2018) 731–743.e712.
- [25]. Reilly SM, Ahmadian M, Zamarron BF, Chang L, Uhm M, Poirier B, Peng X, Krause DM, Korytnaya E, Neidert A, Liddle C, Yu RT, Lumeng CN, Oral EA, Downes M, Evans RM, Saltiel AR, A subcutaneous adipose tissue-liver signalling axis controls hepatic gluconeogenesis, Nat Commun, 6 (2015) 6047. [PubMed: 25581158]
- [26]. Hopkins AL, Keserue GM, Leeson PD, Rees DC, Reynolds CH, The role of ligand efficiency metrics in drug discovery, Nat. Rev. Drug Discovery, 13 (2014) 105–121. [PubMed: 24481311]
- [27]. Freeman-Cook KD, Hoffman RL, Johnson TW, Lipophilic efficiency: the most important efficiency metric in medicinal chemistry, Future Med. Chem, 5 (2013) 113–115. [PubMed: 23360135]
- [28]. Hill AP, Young RJ, Getting physical in drug discovery: a contemporary perspective on solubility and hydrophobicity, Drug Discovery Today, 15 (2010) 648–655. [PubMed: 20570751]
- [29]. Reilly SM, Chiang SH, Decker SJ, Chang L, Uhm M, Larsen MJ, Rubin JR, Mowers J, White NM, Hochberg I, Downes M, Yu RT, Liddle C, Evans RM, Oh D, Li P, Olefsky JM, Saltiel AR, An inhibitor of the protein kinases TBK1 and IKK-varepsilon improves obesity-related metabolic dysfunctions in mice, Nat Med, 19 (2013) 313–321. [PubMed: 23396211]
- [30]. Ma S, He Q, The cyclopropyl effect on the regioselectivity of coupling reactions involving the lithiation of 1-cyclopropyl-2-arylacetylenes, Tetrahedron, 62 (2006) 2769–2778.
- [31]. Brameld KA, Carter DS, Chin E, Javier de Vicente F, Li J, Schoenfeld RC, Sjogren EB, Talamas FX, Heterocyclic antiviral compounds US Patent 8273773 B2 (2012).
- [32]. McCall JM, Romero DL, Kelly RC, Substituted quinoxaline-6-carboxylic acids for the inhibition of PASK, US Patent 8912188 B2 (2014).
- [33]. Spence JTJ, George JH, Structural Reassignment of Cytosporolides A-C via Biomimetic Synthetic Studies and Reinterpretation of NMR Data, Org. Lett, 13 (2011) 5318–5321. [PubMed: 21888334]
- [34]. Ukawa K, Ishiguro T, Kuriki H, Nohara A, Synthesis of the metabolites and degradation products of 2-amino-7-isopropyl-5-oxo-5H-[1]benzopyrano[2,3-b]pyridine-3-carboxylic acid (amoxanox), Chem. Pharm. Bull, 33 (1985) 4432–4437. [PubMed: 3841502]

- [35]. Li D, Han X, Tu Q, Feng L, Wu D, Sun Y, Chen H, Li Y, Ren Y, Wan J, Structure-based design and synthesis of novel dual-target inhibitors against cyanobacterial fructose-1,6-bisphosphate aldolase and fructose-1,6-bisphosphatase, *J. Agric. Food Chem*, 61 (2013) 7453–7461. [PubMed: 23889687]
- [36]. Abdel-Rahman AH, Hammouda MAA, El-Desoky SI, Synthesis of some new azole, azepine, pyridine, and pyrimidine derivatives using 6-hydroxy-4H-4-oxo[1]-benzopyran-3-carboxaldehyde as a versatile starting material, *Heteroat. Chem*, 16 (2005) 20–27.
- [37]. Larabi A, Devos JM, Ng S-L, Nanao MH, Round A, Maniatis T, Panne D, Crystal Structure and Mechanism of Activation of TANK-Binding Kinase 1, *Cell Rep*, 3 (2013) 734–746. [PubMed: 23453971]
- [38]. Tu D, Zhu Z, Zhou AY, Yun C.-h., Lee K-E, Toms AV, Li Y, Dunn GP, Chan E, Thai T, Yang S, Ficarro SB, Marto JA, Jeon H, Hahn WC, Barbie DA, Eck MJ, Structure and Ubiquitination-Dependent Activation of TANK-Binding Kinase 1, *Cell Rep*, 3 (2013) 747–758. [PubMed: 23453972]
- [39]. Kabsch W, XDS, *Acta Crystallogr D Biol Crystallogr*, 66 (2010) 125–132. [PubMed: 20124692]
- [40]. Adams PD, Afonine PV, Bunkoczi G, Chen VB, Davis IW, Echols N, Headd JJ, Hung L-W, Kapral GJ, Grosse-Kunstleve RW, McCoy AJ, Moriarty NW, Oeffner R, Read RJ, Richardson DC, Richardson JS, Terwilliger TC, Zwart PH, PHENIX: a comprehensive Python-based system for macromolecular structure solution, *Acta Crystallogr D Biol Crystallogr*, 66 (2010) 213–221. [PubMed: 20124702]
- [41]. Emsley P, Cowtan K, Coot: model-building tools for molecular graphics, *Acta Crystallogr D Biol Crystallogr*, 60 (2004) 2126–2132. [PubMed: 15572765]
- [42]. Chen VB, Arendall WB, 3rd, Headd JJ, Keedy DA, Immormino RM, Kapral GJ, Murray LW, Richardson JS, Richardson DC, MolProbity: all-atom structure validation for macromolecular crystallography, *Acta Crystallogr D Biol Crystallogr*, 66 (2010) 12–21. [PubMed: 20057044]
- [43]. DeLano W, The PyMOL Molecular Graphics System, DeLano Scientific, San Carlos, CA, 2002.

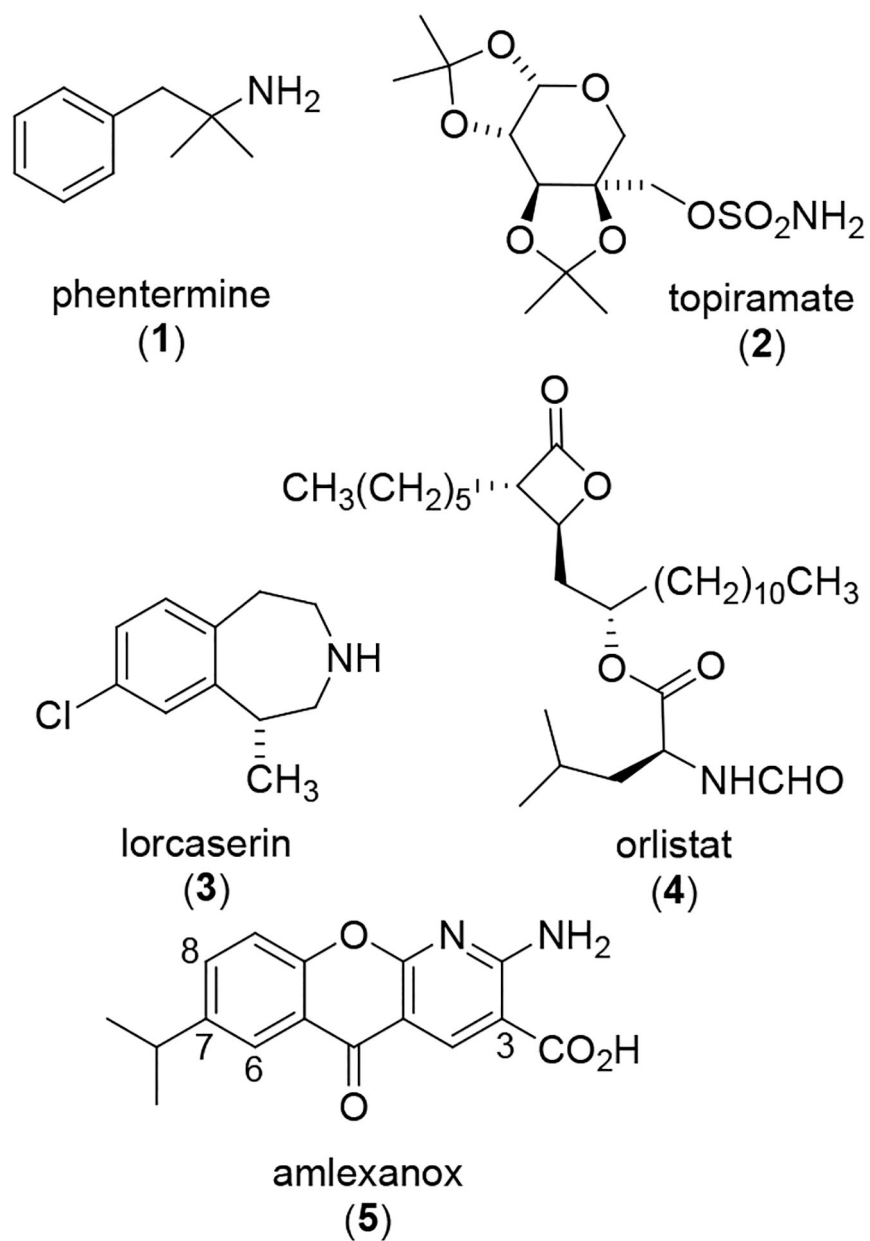


Figure 1.
Structures of anti-obesity drugs

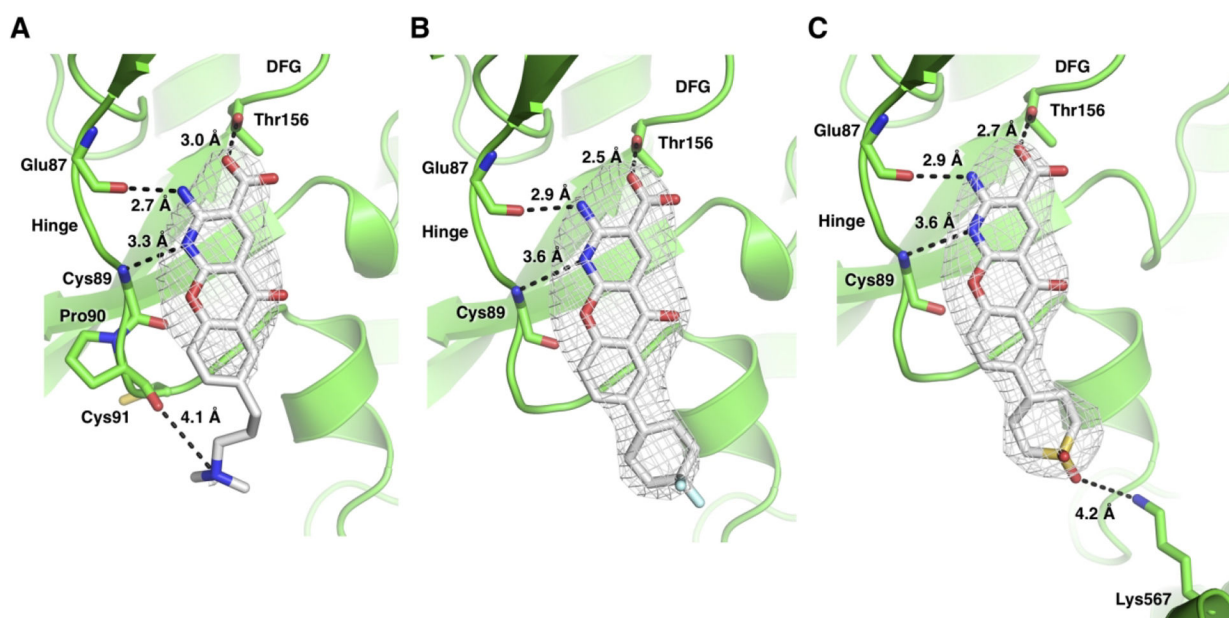


Figure 2:

TBK1 co-crystal structures with analogues (A) **114**, (B) **131**, and (C) **150**. Mesh represents positive $|F_o| - |F_c|$ omit density contoured at 3σ . The amino pyridine portion of the inhibitor core interacts with the backbone of Glu87 and Cys89 in the hinge of the kinase and the carboxylate with Thr156 adjacent to the DFG motif. The structures have been deposited as PDB entries 6CQ0, 6CQ4, and 6CQ5, respectively.

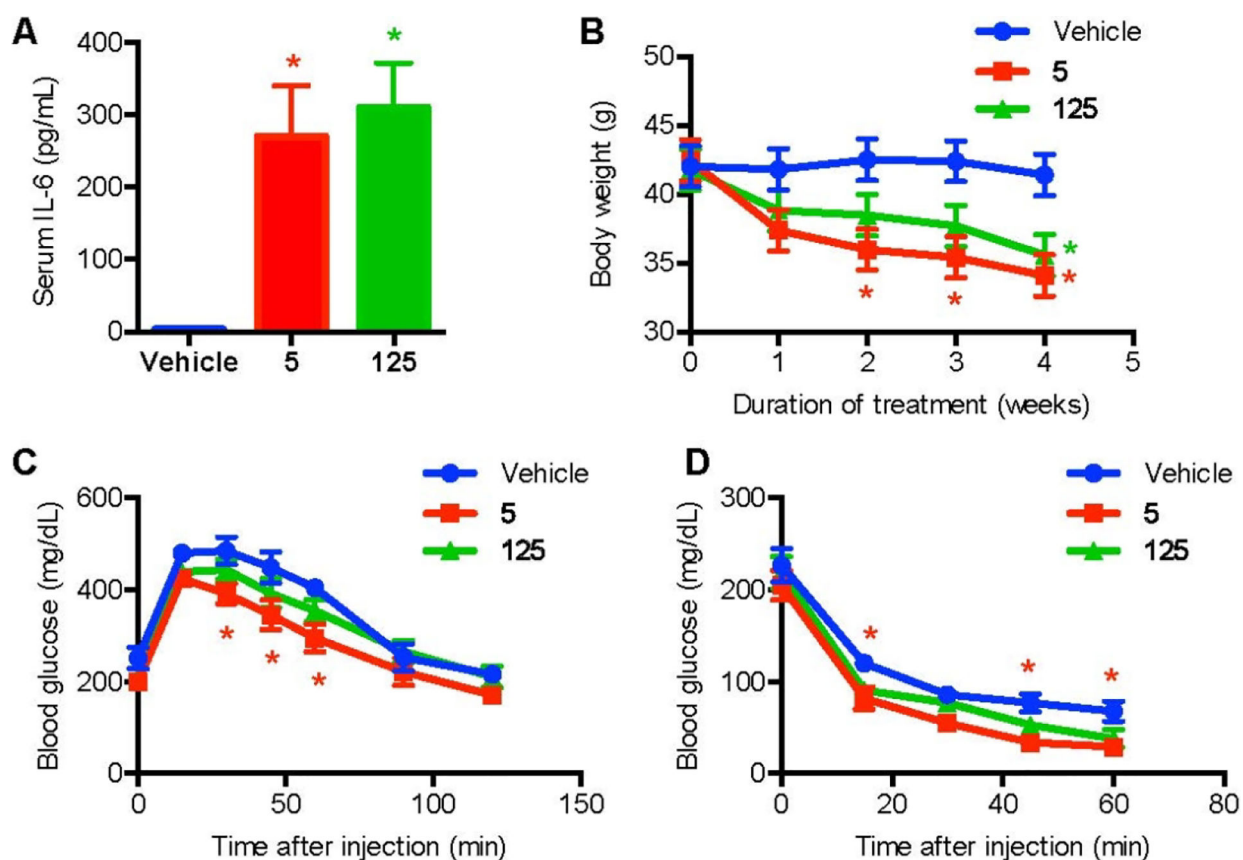
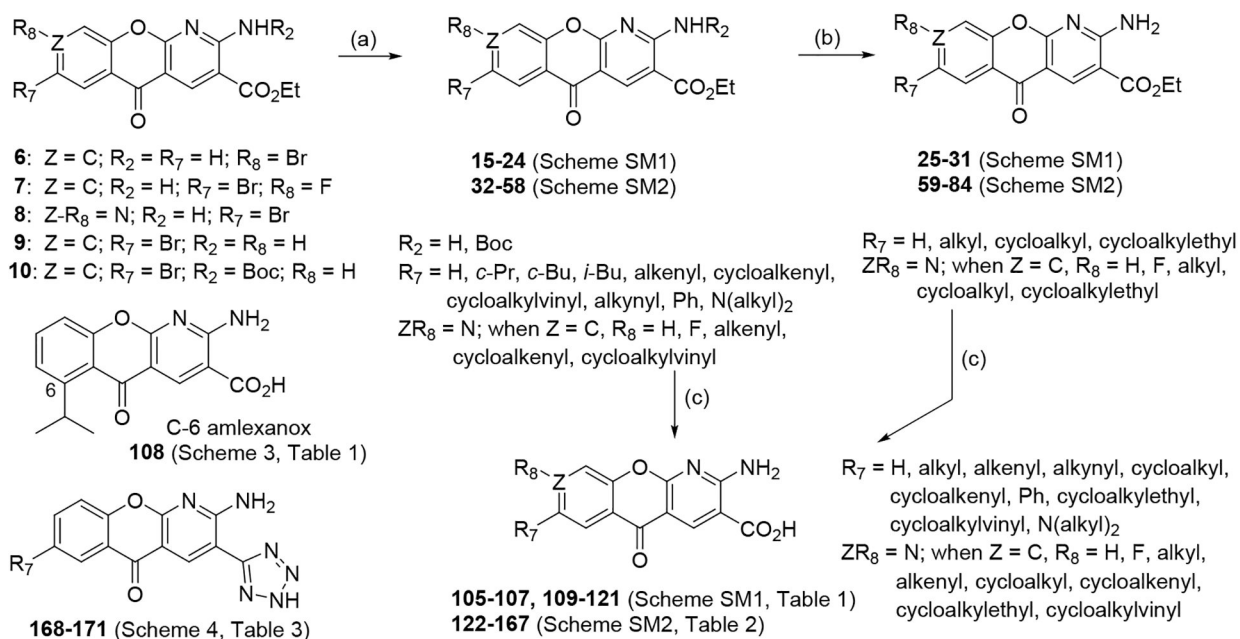


Figure 3:

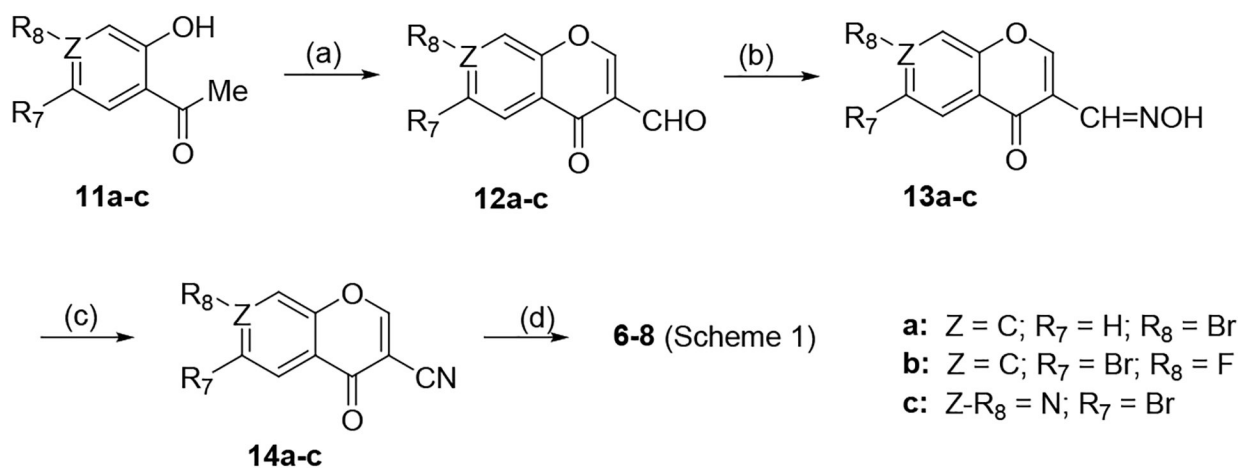
In vivo efficacy of **125** relative to amlexanox (**5**) and vehicle control in a 4-week trial.

Animals were treated by daily oral gavage with 25 mg/kg, (n = 7 per treatment group). This sample size was calculated to be sufficient to detect a significant IL-6 response relative to vehicle (if efficacy is at least 50% of amlexanox), and a 50% change in IL-6 response relative to amlexanox at a power level of 0.80. **A)** Serum IL-6 response after 6 h of treatment. **B)** Body weight over the 4-week treatment period. **C)** Glucose tolerance test after 3 weeks of treatment. **D)** Insulin tolerance test after 4 weeks of treatment. Statistical significance calculated using a one-way ANOVA and two-way ANOVA (time being the second factor), with a Holm-Sidak calculation of significance adjusted for multiple comparisons. * indicates a p -value < 0.05 versus vehicle (red for **5** and green for **125**).

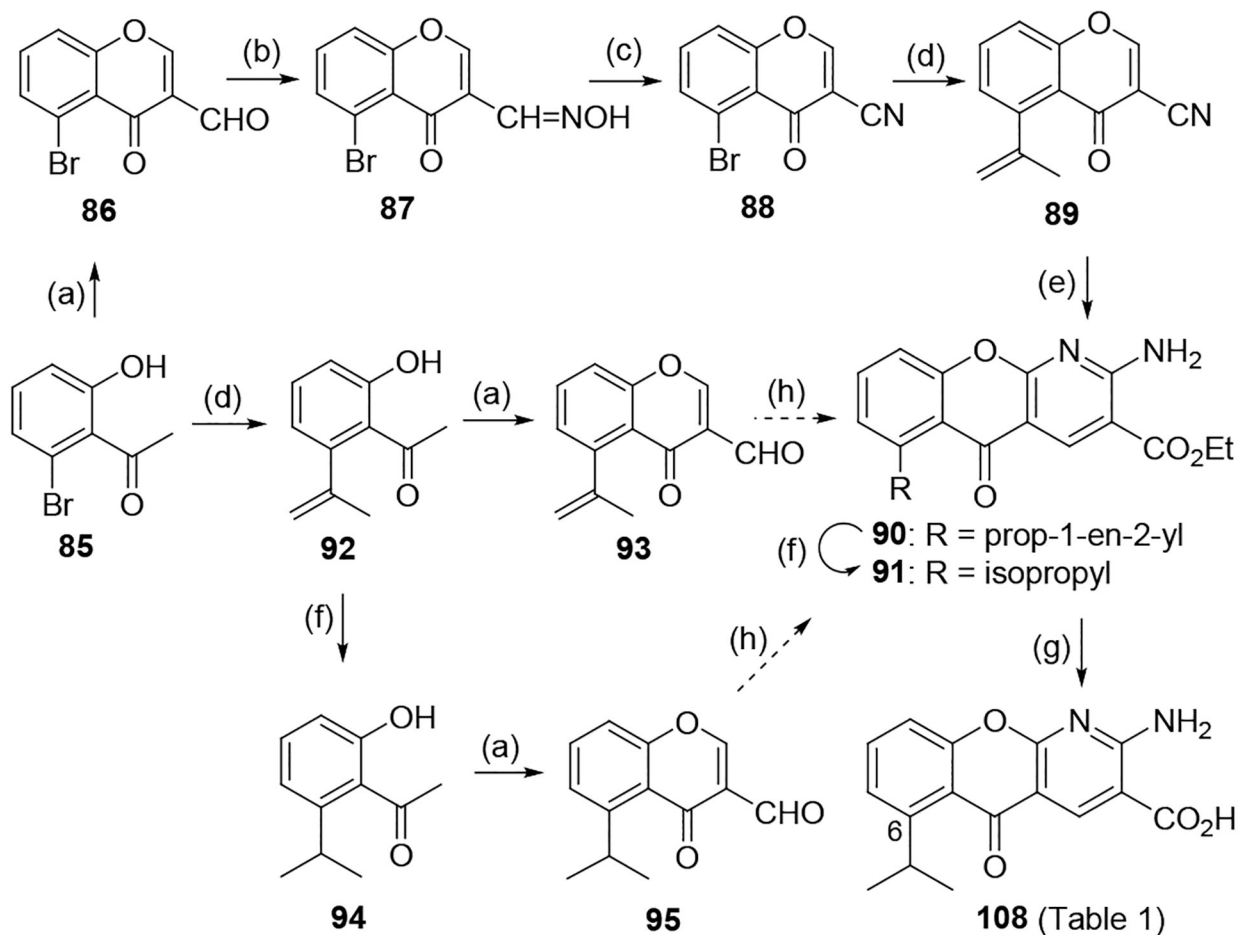


Scheme 1.

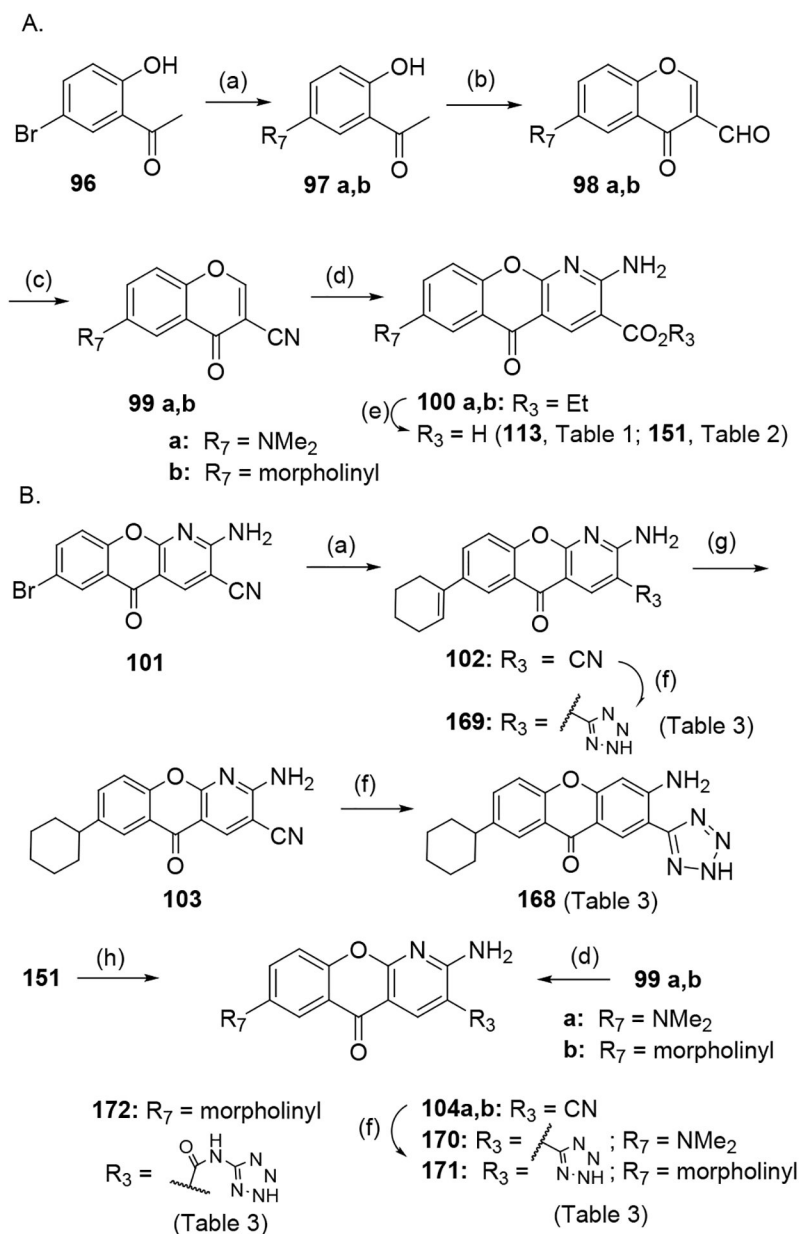
Synthetic strategy to make linear and cyclic amlexanox analogues. (a) Palladium-catalyzed cross coupling reactions. (b) Catalytic hydrogenation. (c) Base hydrolysis. For full details, see Schemes 2–4;

**Scheme 2.**

Synthesis of bromo tricyclic precursors **6-8**. (a) Method I: for **11a,b** to **12a,b**: DMF, POCl₃, 25 °C, 17 h, then H₂O, 73–88%; for **11c** to **12c**: *t*-BuOCH(NMe₂)₂, 25 °C, 17 h, 60% yield; DMF/(CF₃SO₂)₂O, 25 °C, 3 h, then H₂O, 88%. (b) Method J: NH₂OH·HCl, EtOH, 60 °C, 1–2 h, 61–80%. (c) Method K: Ac₂O, 110 °C, 18 h, 94–99%. (d) Method L: CNCH₂CO₂Et, piperidine, EtOH, reflux, 2 h, 77–93%.

**Scheme 3.**

Synthesis of C-6 amlexanox **108**. (a) Method I: DMF, POCl₃, 25 °C, 17 h, then H₂O, 67 – 94%. (b) Method J: NH₂OH·HCl, EtOH, 60 °C, 1 h, 77%. (c) Method K: Ac₂O, 110 °C, 18 h, 99%. (d) Method A: for **88** to **89**: tri-*n*-butyl(prop-1-en-2-yl)stannane, Pd(PPh₃)₂Cl₂, *p*-dioxane, 80–100 °C, 16.5 h, 81%; for **85** to **92**: potassium trifluoro(prop-1-en-2-yl)borate, Pd(PPh₃)₂Cl₂, PPh₃, K₂CO₃, THF, 100 °C, 18 h, 98%. (e) Method L: CNCH₂CO₂Et, piperidine, EtOH, reflux, 2 h, 73%. (f) Method D: H₂, 10% Pd/C, 2:1 v/v EtOH:DCM, 25 °C, 18–45 h, 78 – 95%. (g) Method E: 1N aq NaOH, EtOH, 50 °C, 1.5 h, 86%. (h) Oximation (Method J) results in destruction of starting compound.

**Scheme 4.**

Synthesis of R₇ amino and R₃ tetrazole amlexanox analogues (a) Method A: for **96** to **97a,b**; LiHMDS, NHMe₂ or morpholine; Pd₂(dba)₃, DavePhos, THF, 75 – 80 °C, 1–2 h, 81–100%; for **101** to **102**; 2-(cyclohex-1-en-1-yl)-4,4,5,5-tetramethyl-1,3,2-dioxaborolane, PPh₃, Pd(OAc)₂, K₃PO₄, aq. *p*-dioxane, 70 °C, 1.5 h, 78%. (b) Method I: DMF, POCl₃, 25 °C, 17 h, then H₂O, 68%. (c) Method K: NH₂OH·HCl, NaI, CH₃CN, reflux, 2–3 h, 34–58% yield. (d) Method L: for **99a,b** to **100a,b**: CNCH₂CO₂Et, piperidine, EtOH, reflux, 2.5–4 h, 9–58%; for **99a,b** to **104a,b**: CNCH₂CN, piperidine, EtOH, reflux, 3 h, 65–71%. (e) Method E: 1N aq NaOH, EtOH, 50 °C, 2 h, 85–91% yield. (f) Method M: NaN₃, NH₄Cl, DMF, 90 °C, 16–18 h, 27–84%. (g) Method D: H₂, 10% Pd/C, 47:53 v/v EtOH:DCM,

25 °C, 22 h, 75%. (h) Method N: SOCl_2 / cat. DMF, DCM, reflux, 3 h, and then 5-aminotetrazole, pyridine, NEt_3 , RT, 4h, 38%.

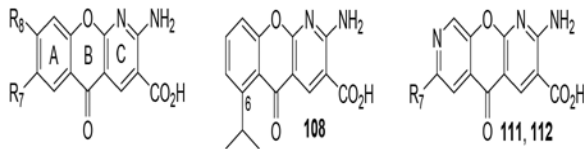
Author Manuscript

Author Manuscript

Author Manuscript

Author Manuscript

Table 1.

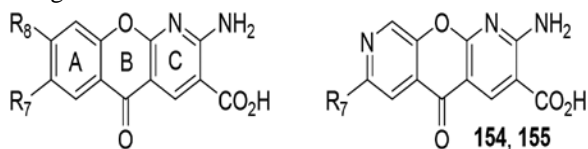
In Vitro Activity of R6 – R8 Linear 5-Oxo-5*H*[1]benzopyrano[2,3-*b*]pyridines and A-ring Aza Congeners.

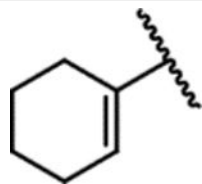
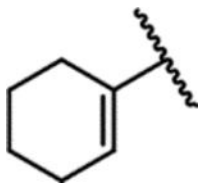
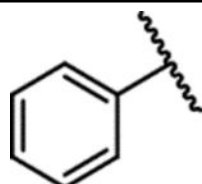
No.	R ₇	R ₈	Single Concentration, % Inhibition) ^a (IC ₅₀ , μM) ^b			
			TBK1	Fold Change IC ₅₀ ^e	IKKe	Fold Change IC ₅₀ ^e
5	<i>i</i> Pr	H	50 ± 1.3 (0.85 ± 0.14)		29 ± 7.4 (5.1 ± 1.6)	
105	CH ₂ =C(CH ₃)-	H	(1.3 ± 0.1 ^c)	0.7	(1.3 ± 0.5 ^d)	3.9
106	H	<i>i</i> Pr	(0.30 ± 0.03 ^d)	2.8	(4.7 ± 2.3)	1.1
107	H	CH ₂ =C(CH ₃)-	(2.3 ± 0.1 ^d)	0.4	(7.2 ± 2.0)	0.7
108	-	-	(1.1 ± 0.02 ^d)	0.8	(6.0 ± 0.5)	0.9
109	<i>i</i> Pr	F	(0.40 ± 0.08)	2.1	(5.4 ± 0.7)	0.9
110	CH ₂ =C(CH ₃)-	F	(0.79 ± 0.07)	1.1	(1.7 ± 0.3 ^c)	3.0
111	<i>i</i> Pr	-	(0.57 ± 0.02 ^d)	1.5	(3.1 ± 1.1)	1.6
112	CH ₂ =C(CH ₃)-	-	(2.0 ± 0.3 ^c)	0.4	(5.3 ± 0.5)	1.0
113	Me ₂ N	H	53 ± 3.4 (0.40 ± 0.09) ^c	2.1	35 ± 3.8 (1.6 ± 0.5)	3.2
114	Me ₂ N(CH ₂) ₃ -	H	35 ± 2.2		21 ± 1.8	
115	Me ₂ NCH ₂ C=C-	H	20 ± 3.4		17 ± 2.0	
116	<i>i</i> Bu	H	(0.55 ± 0.08)	1.5	(4.9 ± 2.0)	1.0
117	<i>i</i> pentyl	H	(0.83 ± 0.08)	1.0	(3.4 ± 0.4)	1.5
118	(CH ₃) ₂ CHC≡C-	H	(12 ± 1 ^c)	0.1	(20 ± 9)	0.3
119	<i>i</i> pentyl	F	32 ± 0.7		-5.7 ± 4.7	
120	<i>i</i> BuCH ₂ CH ₂	H	14 ± 4.8		0.6 ± 11	
121	<i>i</i> BuCH=CH-	H	8.7 ± 4.2		-3.1 ± 3.2	

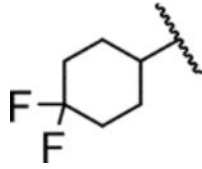
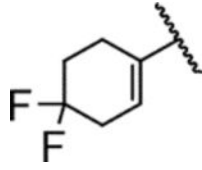
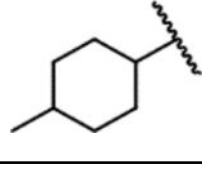
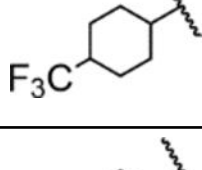
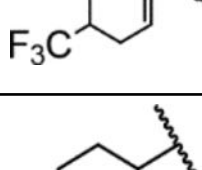
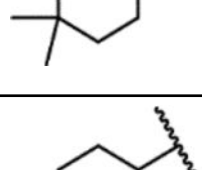
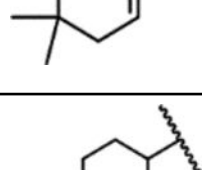
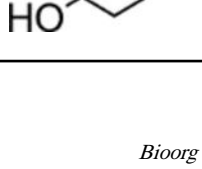
^a TBK1, (1 μM); IKKe (5 μM).^b Concentration for 50% inhibition in radiometric kinase assays using purified protein. Reported as IC₅₀ (μM) ± SEM (n=3). Significance relative to amlexanox determined by a two-tailed Student's T-test (^c p<0.05,^d p<0.01.^e Fold change over amlexanox (5) calculated from the mean IC₅₀ values. See Experimental Section.

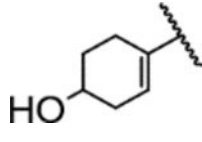
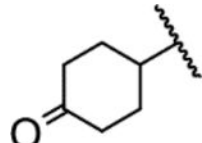
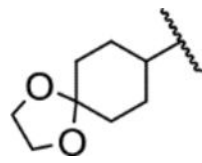
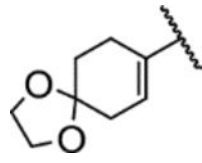
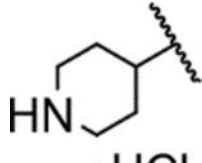
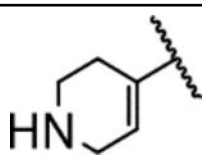
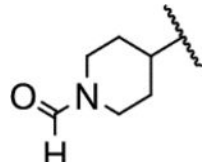
Table 2.

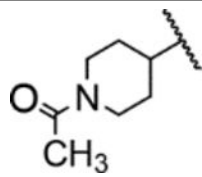
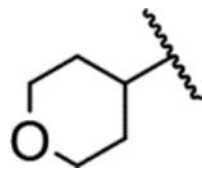
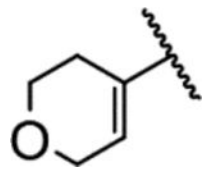
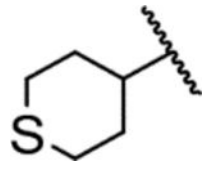
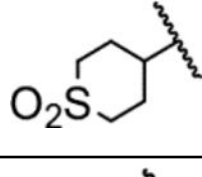
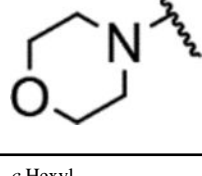
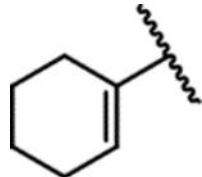
In Vitro Activity of R7 and R8 Cycloalkyl, Heterocyclic and Alkylcycloalkyl 5-Oxo-5*H*-[1]benzopyrano[2,3-*b*]pyridines and A-ring Aza Congeners.

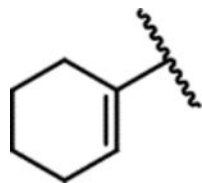
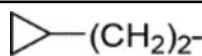
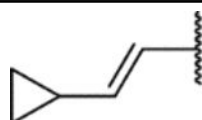
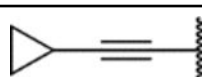
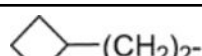
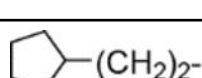
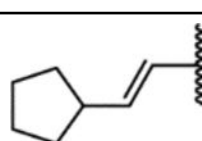
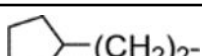
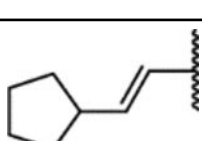
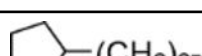
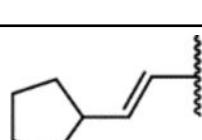


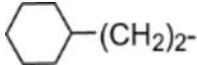
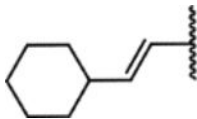
No.	R ₇	R ₈	Single Concentration, % Inhibition) ^a (IC ₅₀ , μM) ^b			
			TBK1	Fold Change ^e	IKKe	Fold Change ^e
5	<i>i</i> -Pr	H	50 ± 1.3 (0.85 ± 0.14)		29 ± 7.4 (5.1 ± 1.6)	
122	<i>c</i> -Pr	H	(2.3 ± 0.1) ^d	0.4	(10.6 ± 0.4) ^d	0.5
123	<i>c</i> -Bu	H	44 ± 3.7 (4.6 ± 3.6)	0.2	25 ± 3.4 (3.1 ± 0.7) ^c	1.6
124	<i>c</i> -Pentyl	H	67 ± 4.1 (1.8 ± 0.3) ^c	0.5	9.2 ± 1.9 (6.3 ± 1.0)	0.8
125	<i>c</i> -Hexyl	H	34 ± 1.6 (1.9 ± 0.6)	0.5	9.0 ± 3.1 (>100)	
126		H	44 ± 0.2 (1.7 ± 0.5)		41 ± 4.9 (5.4 ± 1.5)	
				0.5		0.9
127	<i>c</i> -Heptyl	H	32 ± 8.5		9.2 ± 4.1	
128	H	<i>c</i> -Hexyl	11 ± 9.6		8.2 ± 6.3	
129	H		15 ± 3.7		15 ± 4.7	
130		H	34 ± 2.9		33 ± 6.4	

No.	R ₇	R ₈	Single Concentration, % Inhibition) ^a (IC ₅₀ , μM) ^b			
			TBK1	Fold Change ^e	IKKe	Fold Change ^e
131		H	14 ± 3.8		11 ± 2.1	
132		H	27 ± 3.8		19 ± 5.6	
133		H	19 ± 5.6		3.2 ± 2.9	
134		H	33 ± 8.0		11 ± 2.3	
135		H	4.0 ± 4.0		0.4 ± 0.4	
136		H	15 ± 6.5		-0.7 ± 7.5	
137		H	38 ± 4.5		22 ± 2.4	
138		H	37 ± 2.8		12 ± 2.2	

No.	R ₇	R ₈	Single Concentration, % Inhibition) ^a (IC ₅₀ , μM) ^b			
			TBK1	Fold Change ^e	IKKe	Fold Change ^e
139		H	27 ± 2.8		26 ± 3.6	
140		H	52 ± 6.2 (0.45 ± 0.07 ^c)	1.9	27 ± 4.9 (1.5 ± 1.3)	3.4
141		H	63 ± 1.1 (0.44 ± 0.05 ^c)	1.9	30 ± 8.1 (3.2 ± 0.03 ^d)	1.6
142		H	54 ± 2.4 (0.75 ± 0.06)	1.1	63 ± 4.6 (2.1 ± 0.8 ^c)	2.4
143		H	12 ± 8.7		7.9 ± 8.6	
144		H	22 ± 3.4		23 ± 2.7	
145		H	68 ± 1.1 (0.49 ± 0.05 ^c)	1.7	34 ± 8.4 (5.2 ± 2.9)	1.0

No.	R ₇	R ₈	Single Concentration, % Inhibition) ^a (IC ₅₀ , μM) ^b			
			TBK1	Fold Change ^e	IKKe	Fold Change ^e
146		H	66 ± 1.3 (0.27 ± 0.03 ^d)	3.1	26 ± 7.5 (1.9 ± 2.6)	2.7
147		H	46 ± 0.4 (0.75 ± 0.22)	1.1	32 ± 13 (11 ± 5.5)	0.5
148		H	46 ± 4.0 (0.86 ± 0.56)	1.0	50 ± 2.3 (2.0 ± 0.6 ^c)	2.6
149		H	46 ± 1.8 (0.29 ± 0.10 ^c)	2.9	18 ± 2.5 (1.2 ± 0.4 ^d)	4.3
150		H	57 ± 4.1 (0.83 ± 0.12)	1.0	23 ± 2.3 (11 ± 6.7)	0.5
151		H	32 ± 5.9		3.5 ± 10	
152	c-Hexyl	F	26 ± 8.4		8.2 ± 3.0	
153		F	10 ± 6.8		-0.5 ± 1.3	
154	c-Hexyl	-	14 ± 4.9		7.0 ± 1.1	

No.	R ₇	R ₈	Single Concentration, % Inhibition) ^a (IC ₅₀ , μM) ^b			
			TBK1	Fold Change ^e	IKKe	Fold Change ^e
155		-	-1.2 ± 6.6		3.0 ± 1.4	
156		H	31 ± 6.0		7.7 ± 1.9	
157		H	29 ± 4.8		10 ± 6.8	
158		H	11 ± 3.2		-6 ± 8.0	
159		H	26 ± 4.9		8.7 ± 6.8	
160		H	3.2 ± 10		4.8 ± 5.5	
161		H	44 ± 1.0		13 ± 4.6	
162	H		4.7 ± 7.1		5.2 ± 2.0	
163	H		8.8 ± 2.5		6.5 ± 2.3	
164		F	-4.4 ± 7.2		-7.1 ± 4.0	
165		F	2.9 ± 3.2		-0.2 ± 2.4	

No.	R ₇	R ₈	Single Concentration, % Inhibition) ^a (IC ₅₀ , μM) ^b			
			TBK1	Fold Change ^e	IKKe	Fold Change ^e
166		H	-1.9 ± 2.3		-4.1 ± 3.7	
167		H	13 ± 1.3		4.3 ± 0.7	

^a TBK1, (1 μM); IKKμ (5 μM).

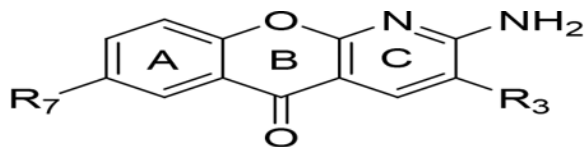
^b Concentration for 50% inhibition in radiometric kinase assays using purified protein. Reported as IC₅₀ (μM) ± SEM (n=3). Significance relative to amlexanox determined by a two-tailed Student's T-test (

^c p<0.05,

^d p<0.01.

^e Fold change over amlexanoc (5) calculated from the mean IC₅₀ values. See Experimental Section.

Table 3.

In Vitro Activity of R₃, R₇ Disubstituted 5-Oxo-5*H*-[1]benzopyrano[2,3-*b*]pyridines

No.	R ₃	R ₇	Single Concentration % Inhibition ^a (IC ₅₀ , μM) ^b			
			TBK1	Fold Change ^f	IKKe	Fold Change ^f
5	CO ₂ H	<i>i</i> -Pr	50 ± 1.3 (0.85 ± 0.14)		29 ± 7.4 (5.1 ± 1.6)	
168		<i>c</i> -Hexyl	64 ± 1.5 (1.9 ± 0.2 ^c)	0.4	30 ± 2.2 (1.0 ± 0.3 ^c)	5.1
169			52 ± 3.3 (0.49 ± 0.05 ^c)	1.7	79 ± 2.1 (0.21 ± 0.06 ^e)	24
170		Me ₂ N	33 ± 0.6 (0.53 ± 0.16)	1.6	65 ± 1.3 (0.58 ± 0.2 ^e)	8.8
171			34 ± 3.6 (0.54 ± 0.10)	1.6	70 ± 1.1 (0.31 ± 0.14 ^e)	16
172			49 ± 0.5 (0.76 ± 0.11)	1.1	57 ± 1.7 (1.2 ± 0.4 ^d)	4.3

^a TBK1, (1 μM); IKKe (5 μM).^b Concentration for 50% inhibition in radiometric kinase assays using purified protein. Reported as IC₅₀ (μM) ± SEM (n=3). Significance relative to amlexanox determined by a two-tailed Student's T-test (

^c
p<0.05,

^d
p<0.01,

^e
p<0.001).

^f
Fold change over amlexanoc (**5**) calculated from the mean IC₅₀ values. See Experimental Section.

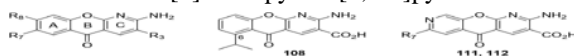
Author Manuscript

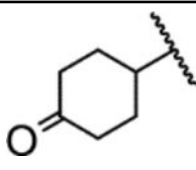
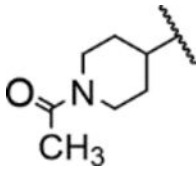
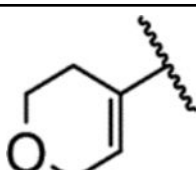
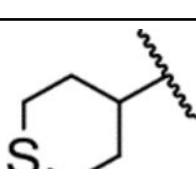
Author Manuscript

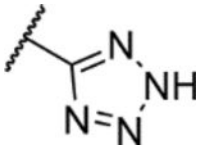
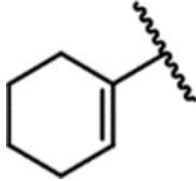
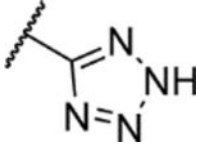
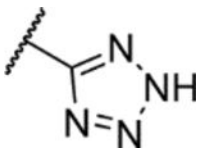
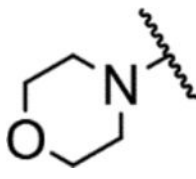
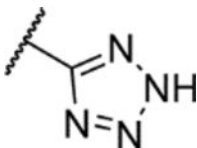
Author Manuscript

Author Manuscript

Table 4.

Cellular Activity of Synthesized 5-Oxo-5*H*-[1]benzopyrano[2,3-*b*]pyridines and A-ring Aza Congeners.

No.	R ₇	R ₈	R ₃	p38 T180/Y182 ^a	pTBK1 S172 ^a	IL-6 secretion ^b
5	<i>i</i> Pr	H	CO ₂ H	1.00	1.00	1.00
105	CH ₂ =C(CH ₃)-	H	CO ₂ H	0.48	1.42	1.11
106	H	<i>i</i> Pr	CO ₂ H	0.96	1.23	0.96
107	H	CH ₂ =C(CH ₃)-	CO ₂ H	0.79	0.52	0.20
108	-	-	CO ₂ H	1.80	1.20	2.33
109	<i>i</i> Pr	F	CO ₂ H	0.93	1.30	1.36
110	CH ₂ =C(CH ₃)-	F	CO ₂ H	0.41	0.61	1.20
111	<i>i</i> Pr	-	CO ₂ H	0.03	0.04	0.19
112	CH ₂ =C(CH ₃)-	-	CO ₂ H	0.03	0.04	0.22
113	Me ₂ N	H	CO ₂ H	0.47	0.23	0.48
116	<i>i</i> Bu	H	CO ₂ H	1.4	0.46	2.56
117	<i>i</i> Pentyl	H	CO ₂ H	0.7	3.40	2.46
118	(CH ₃) ₂ CHC≡C-	H	CO ₂ H	0.8	0.20	0.42
125	<i>o</i> -Hexyl	H	CO ₂ H	1.33	3.44	3.58
140		H	CO ₂ H	0.00	n.d.	0.07
146		H	CO ₂ H	0.60	0.29	0.33
148		H	CO ₂ H	0.59	1.27	1.53
149		H	CO ₂ H	1.19	1.54	1.55

No.	R ₇	R ₈	R ₃	p38 T180/Y182 ^a	pTBK1 S172 ^a	IL-6 secretion ^b
168	c-Hexyl	H		0.49	n.d.	0.17
169		H		0.10	n.d.	0.00
170	Me ₂ N	H		0.00	n.d.	0.03
171		H		0.70	0.39	0.54

^aPhosphorylation of p38 or TBK1 in 3T3-L1 adipocytes treated with 100 μM compound normalized to the response to amlexanox (5). Values are determined from a single experiment with technical duplicates.

^bIL-6 secretion (pg/mL) from 3T3-L1 adipocytes treated with 100 μM compound normalized to the response to amlexanox (5). Values are determined from a single experiment with technical triplicates.

^cn.d.: not determined.